Flexible ligands in heterogeneous catalysts for olefin polymerization: Insights from spectroscopy

Flexible ligands in heterogeneous catalysts for olefin polymerization: insights from spectroscopy

Alessandro Piovano,* Elena Groppo

Department of Chemistry, NIS Centre and INSTM, University of Torino, via Giuria 7, 10125 Torino, Italy

Abstract

Heterogeneous catalysis for olefin polymerization is one of the most relevant industrial processes in terms of worldwide diffusion, material volume, and economic turnover. At the base of this process, two main families of multicomponent catalysts, the Ziegler-Natta and the Phillips ones, which have been developed independently since the 1950s and nowadays serve different sectors of the market. This review aims at unifying the picture of these catalysts, pointing out the often-neglected relevance of the ligands around the active sites, including not only the additives explicitly included in the general composition, but also some compounds that are generated in situ during the catalytic process by side reactions, and even the support material itself. All these components have a direct influence on the properties of the catalytic sites and, in turn, on the overall activity and on the properties of the produced polymers. A multi-technique spectroscopic investigation has the potential to shed light on the fleeting, but decisive interactions among all the components and their effect on the catalytic active sites, contributing to create a proper three-dimensional (nano-sized) environment and acting in a concerted way during the olefin polymerization. A few spectroscopic results obtained in our lab are reported, in order to show in parallel how the same principles of coordination chemistry can be effectively applied to both Ziegler-Natta and Phillips catalysts.

1. Homogeneous and heterogeneous catalysts for olefin polymerization: a unifying picture

The chemical process of olefin polymerization is a very dynamic field, continuously expanding since the almost simultaneous discovery of Ziegler-Natta and Phillips catalysts in the 1950s, with further pulses at almost regular intervals of about twenty years because of the successive discoveries of the homogeneous metallocene and post-metallocene catalysts [1-6]. Nowadays, the worldwide polyolefins market hovers around 300 billion dollars per year, with the perspective to increase by a further 50% over the next 5 years [7]. At a difference to other sectors of industrial catalysis dominated by a single catalyst with unrivaled performances in terms of activity and/or selectivity, in olefin polymerization catalysis homogeneous and heterogeneous catalysts are co-

present on the scene and satisfy different needs of the market, so that they can be considered as complementary to each other rather than competing [2]. Starting from the same simple monomers (ethylene, propylene and α-olefins) and typically exploiting the same Cossee-Arlman 1,2-insertion mechanism [8], each catalyst produces its own characteristic polymer differing in terms of molecular weight (M_w), molecular weight distribution (MWD), comonomer incorporation and distribution, branching degree and length of the branches, stereoselectivity, regioselectivity and block-structure [6, 9]. In turn, the polymer architecture at a molecular scale influences the macroscopic properties of the whole material, such as the mechanical, rheological and thermal behavior [10].

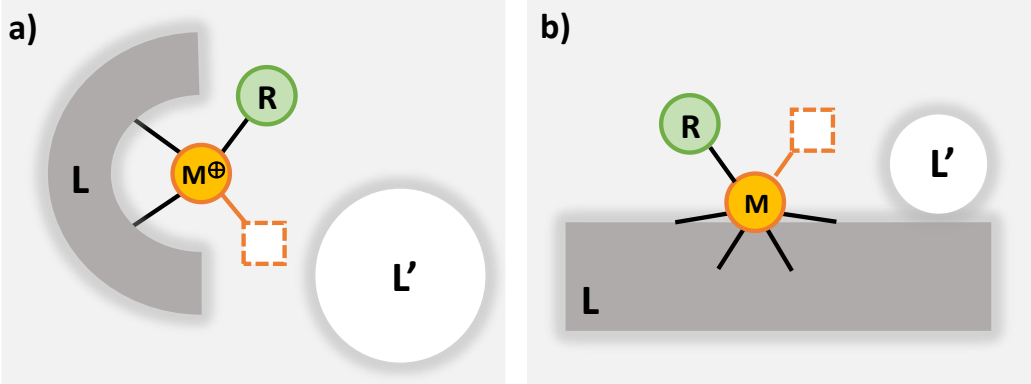

Figure 1. Schematic representation of the key-elements in homogeneous (part a) and heterogeneous (part b) catalysts for olefin polymerization. $M^{\oplus}$ or M = transition metal (the active site); R = alkyl chain (usually a methyl group in homogeneous catalysis); dashed square = coordination vacancy; L = strongly bonded ligand; L' = additional ligand in non-covalent interaction with the $M^{\oplus}$ or M site (usually $MAO^{\ominus}$ in homogeneous catalysis).

For homogeneous olefin polymerization catalysis, it is widely accepted that such a versatility is mainly due to the combination of a few key-elements, which are schematically represented in Figure 1a: 1) a metal cation ($M^{\oplus}$), typically Ti, Zr or Hf for metallocene catalysts and late transition metals (as Ni or Pd) for post-metallocene catalysts; 2) a strongly coordinated (covalently bonded) ligand (L), which provides the appropriate steric and electronic environment around the central metal; 3) a coordination vacancy, necessary for the coordination of olefin; 4) a methyl or alkyl group (R), generated after activation by an alkyl-aluminum compound (usually methyl alumoxane, MAO), which acts as initiator of the polymerization by migrating onto the coordinated olefin; 5) a more or less complex anion (L') in non-covalent interaction with the metal cation (usually the $MAO^{\ominus}$ originated from the reaction of MAO with the organometallic pre-catalyst).

It is well documented that small variations in the structure, geometry and flexibility of the strongly coordinated ligand L could lead to important changes on the active site functionality, on the catalytic performances and on the selectivity [11]. Depending on the type of the ligand, homogeneous catalysts may be conveniently tailored so as to produce polymer chains having a specific length distribution, ranging from a few monomer units to thousands. A paradigmatic example is that of homogeneous nickel catalysts (Figure 2a), where different families can give almost exclusively ethylene oligomers (e.g. Keim's Ni chelate ylides [12, 13]) or tailored polyolefins (e.g. Brookhart's Ni α-diimines [14] and Grubbs' Ni-iminophenolates [15-17]). For example, the Brookhart's Ni α-diimine catalysts can produce tailored polyethylene using ethylene as the only feedstock, through a characteristic chain-walking process [14, 18-20]. Different ligand backbone structures and/or changes in the N-aryl substituents provide various coordination environments and have an influence on the electronic and steric properties of the Ni center. In this way it is possible to tune the chain-walking behavior and control the polyethylene microstructure.

Similarly, single-site metallocene–based catalysts containing a chiral ligand set that induces a "chiral pocket" around the active site, can be tuned to produce selectively isotactic, syndiotactic, hemiisotactic or stereoblock polypropylenes. When the stereochemical regulation of the olefin polymerization process depends on the catalyst, it is referred to as "enantiomorphic site controlled" [21, 22]. In the majority of cases, enantiomorphic site control can be predicted by the symmetry of the metal center (Ewen's symmetry rules) [23, 24]. For example, zirconocene catalysts with C_1 symmetry should produce a hemi–isotactic PP (complex A in Figure 2b), while complexes with a C_s symmetry should produce perfectly syndiotactic PP (complex B in Figure 2b). Nevertheless, Figure 2b shows that the symmetry of the complex is only a part of the puzzle [25-28]. For example, both complexes A and C belong to the C_1 symmetric family of metallocenes, but they produce polymers with different microstructure depending on the steric hindrance of the substituent on the 3–position of the cyclopentadienyl moiety: while complex A produces hemi-isotactic PP as expected, complex C produces isotactic PP. The same delicacy in balancing the steric control can be found for the C_s symmetric family of zirconocenes. For example, complex D possesses all the symmetry and structural requirements of a syndio-specific catalyst, but produces a totally atactic PP because of dynamic interchanges in the ligand conformation, which disrupt the balance of steric forces and stereorigidity.

Besides, also the nature of the anion in non-bonded interaction with the active site has important consequences on the catalyst performances, affecting in particular the coordination

ability of the monomer. Indeed, the initiation of the polymerization process requires the displacement of the anion, so that the olefin can be coordinated. Strongly coordinating anions compete with olefin to occupy the coordination vacancy in *cis* position with respect to the alkyl group (either the initial methyl group or, then, the growing polymeric chain) and consequently the activity of the catalyst is reduced. The mobility of the anion is therefore an important factor and has become the focus of a number of detailed investigations [29-37].

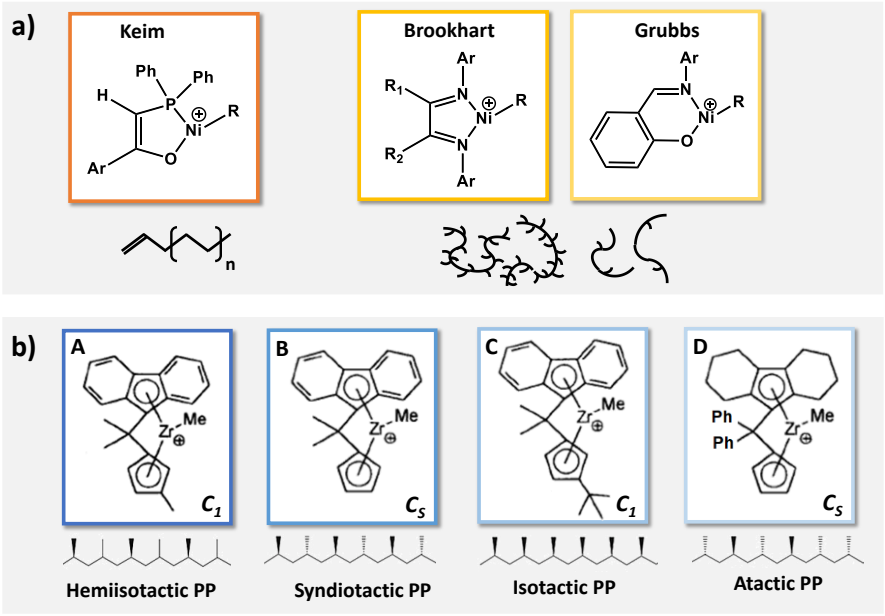

Figure 2. Part a) Representative examples of homogeneous Ni pre-catalysts and of the types of products they produce starting from ethylene as the only feedstock. Part b) Examples of how small changes in the L substituents in zirconocene pre-catalysts drastically affect the type of produced polypropylene.

Much less explored (if not often neglected) is the role of the ligands in heterogeneous catalysis. From a general point of view the structure of heterogeneous catalysts for olefin polymerization can be described in very similar terms as for homogeneous catalysts. Even though the definition of the active sites at a molecular level is still matter of debate in most of the cases, there is a general consensus on that the active phase is constituted by isolated transition metal species, strongly bonded to a support material (which can be considered as a macro-ligand L), with an alkyl chain and a coordination vacancy nearby (as generically depicted in Figure 1b). For Ziegler-Natta (ZN) catalysts, the active metal species (M) is a reduced and alkylated Ti site, which is bonded to a highly disordered δ-$MgCl_2$ support (the macro-ligand, L). The alkyl chain derives from reaction of the $TiCl_4$ precursor with an Al-alkyl activator, usually triethyl-aluminum (TEAl). In addition to these components, modern ZN catalysts also contain electron-donor ligands (L'), which are in non-bonded (or weakly-bonded) interaction with the Ti sites, but play a dominant role in

affecting the stereo-selectivity in propene polymerization. For the Phillips catalyst the active site (M) originates from the in situ reduction and alkylation by the ethylene monomer itself of a mono-chromate ion covalently bonded to amorphous silica (L), during the induction time that precedes the onset of ethylene polymerization. The by-products of the reaction have been recently demonstrated to remain in close interaction with the active Cr sites, and hence they can be classified as L' ligand in our simplified scheme.

Despite the high heterogeneity of the sites in both ZN and Phillips catalysts (it is worth noticing that only a fraction of the metal sites are actually active in the catalysis, most of them are just inactive (dormant, deactivated or spectator) species [38]), in this contribution we will show that also for solid olefin polymerization catalysts the ligands L and L' take an important part in the definition of the properties of the active sites, contributing to create a proper three-dimensional (nano-sized) environment and acting in a concerted way during the olefin polymerization. To this purpose, we have selected a few examples belonging to both the categories of heterogeneous catalysts for olefin polymerization cited above. We will demonstrate that spectroscopic methods have the potential to unravel the coordination chemistry involving the active sites and to decipher the mutual interactions between all the components [38-43]. In particular, we will focus the attention on the ligands L and L', demonstrating that in many cases they display a flexible and dynamic behavior very much similar to that found in homogeneous catalysts. Most of the examples are taken from our own research, although with constant reference to the most significant findings from other research groups. In this, we do not want to overshadow the results by others, but we prefer to rigorously compare results obtained on different catalysts analyzed in the same experimental conditions, which is a condition difficult to fulfill when comparing results obtained in different laboratories. The review does not want to cover the topic in an exhaustive way, but aims at providing some snapshots as food for thoughts, to demonstrate that the borders between homogeneous and heterogeneous catalysis are not so sharp as one can imagine at a first sight.

2.1. Ligands in non-bonding (or weakly-bonding) interaction

2.1.1. The electron donors in Ziegler-Natta catalysts

Modern heterogeneous $MgCl_2$-supported ZN catalysts are highly sophisticated, hierarchical, nano-materials with a complex chemical composition, which is the result of several successive breakthroughs. One of the fundamental steps in ZN catalysts development, which dates back to

the 1960s, was the discovery that the addition to the catalyst composition of some electron-rich organic compounds (also called electron donors) greatly improves the stereospecificity in propene polymerization [9, 44-47]. Since then, most of the industrial research in this field was devoted to the screening of new electron donors and the optimization of their composition [48]. At present, a series of experimental evidences have been accumulated on the fact that the electron donors, added either during the synthesis of the pre-catalyst (internal donors) or together with the Al-alkyl activator (external donors), exert multiple functions, among which: i) control of the morphology of the catalyst particles [49, 50]; ii) regulation of the distribution of the active sites [51-53]; iii) enhancement of the regioselectivity [54-56]; iv) improvement of the comonomer incorporation [57]; v) control of the molecular weight through the hydrogen response [56, 58, 59].

The extraordinary effects of the electron donors on the catalysts' performances explain why a lot of efforts have been devoted to understand their working mechanism at a molecular level. The first model was proposed by Corradini in the late 1970s [60, 61] on the basis of elegant crystallographic considerations, and was broadly accepted for a long time, triggering decades of flawed mechanistic speculation [62]. According to this model, the electron donors interact only with the $MgCl_2$ support and thus contribute to the catalyst stereoselectivity in an indirect way, controlling the distribution of the surface sites suitable for $TiCl_4$ grafting and preventing the formation of aspecific Ti species [61, 63, 64]. This fostered the classification of the $MgCl_2$ surfaces as "good" or "bad", depending on whether they can host the chiral Ti sites or not, and the idea that the electron donors compete with $TiCl_4$ for selective chemisorption on the $MgCl_2$ support. The model started to be questioned when it became impossible to ignore the unambiguous experimental evidences that electron donor molecules have a direct and specific impact on polymer microstructure [51]. Therefore, if not in close interaction with the active sites, the electron donors must be at least in their close proximity, in non-bonded contact with them. The failure of the Corradini model was definitely sanctioned with the advent of modern advanced computational methods, which incontrovertibly demonstrated that the possible $TiCl_x$ species formed on $MgCl_2$ are quite limited and mostly determined by the different strength of interaction between Ti and the exposed surfaces [65-70].

An alternative and drastically opposite model to explain the role of electron donors in ZN catalysis proposes a direct coordination of the electron donors to the Ti chloride species through a coordination vacancy, with the creation of a new active (and stereo-specific) center [45, 71-75]. The model was corroborated by a few IR spectroscopic evidences pointing out the presence of

$TiCl_4$-donor complexes in the liquid reaction mixture during the synthesis of ZN catalysts [76, 77]. The thermodynamics for the complexation of $TiCl_4$ with many organic molecules typically used as electron donors was quantitatively evaluated through calorimetric experiments [78]. In all cases, octahedral Ti complexes with two coordinated oxygen atoms were formed, whereby the two oxygen atoms may come from two separate ligands per metal site for monodentate molecules, or from a single chelating ligand for the bidentate ones. The enthalpy of complex formation correlates with the catalytic efficiency in propylene polymerization in the liquid phase, once that the complex is activated by Al-alkyl. This leads to the conclusion that an optimal electron donor should display a strong affinity for $TiCl_4$ [78]. However, the hypothesis of a direct interaction between the Ti sites and the electron donor molecules is weakened by the finding that the electron donors react with the aluminum alkyls, and they can also be extracted from the catalyst in different amounts [62].

Between the two above mentioned hypotheses a third one, indicated as three-site or co-adsorption model, implies that the electron donor molecules are adsorbed on $MgCl_2$ surface in the near proximity of the Ti sites, but with a non-bonding interaction [53, 62, 68, 79-83]: the different possible configurations of the electron donor molecules at the $MgCl_2$ surface and their flexibility determine a large variety of different stereoselective Ti sites. In this way, the stereospecificity of supported Ti species is described irrespective of their location (on “good” or “bad” $MgCl_2$ surfaces) and nuclearity (mononuclear or dinuclear), but according to the absence or presence of bulky ligands (Cl or donor) at the neighboring undercoordinated metal sites (Mg, Ti, or Al). For instance, cluster DFT calculations firstly proved that the co-adsorption of two succinate molecules can convert the aspecific Ti mononuclear species on the $MgCl_2$ (110) surface into isospecific one [80].

IR spectroscopy has been by far one of the most used experimental technique to investigate the coordination mode of the electron donors in ZN catalysts. Indeed, most of these molecules are characterized by functional groups which display intense absorption bands in the IR spectrum, whose frequency position is highly sensitive to the adsorption mode. For example, benzoates and phthalates, which are two among the most employed internal donors, contain carbonyl groups, which are responsible of an intense band at about 1700 cm^{-1} or below. ZN pre-catalysts synthetized following different protocols have been systematically investigated by IR spectroscopy [84-90]: the ν(C=O) absorption band in the IR spectra is generally broad and can be deconvoluted using multiple components. As a rule of thumb, lower is the energy (i.e., larger is the shift with respect to the pure molecule), stronger is the interaction with the adsorption site (i.e.,

more acidic is the site). Hence, ν(C=O) components at progressively decreasing energy are assigned to the electron donor adsorbed on weak, medium and strong acid sites, respectively. Generally speaking, on $MgCl_2$ surfaces the acid strength of the Mg^{2+} cations increases with lowering their coordination, i.e. $Mg_{5c}^{2+} < Mg_{4c}^{2+} < Mg_{3c}^{2+}$ (the latter corresponding to defect sites). Moreover, a Ti^{4+} site is more acidic than any Mg^{2+} cation.

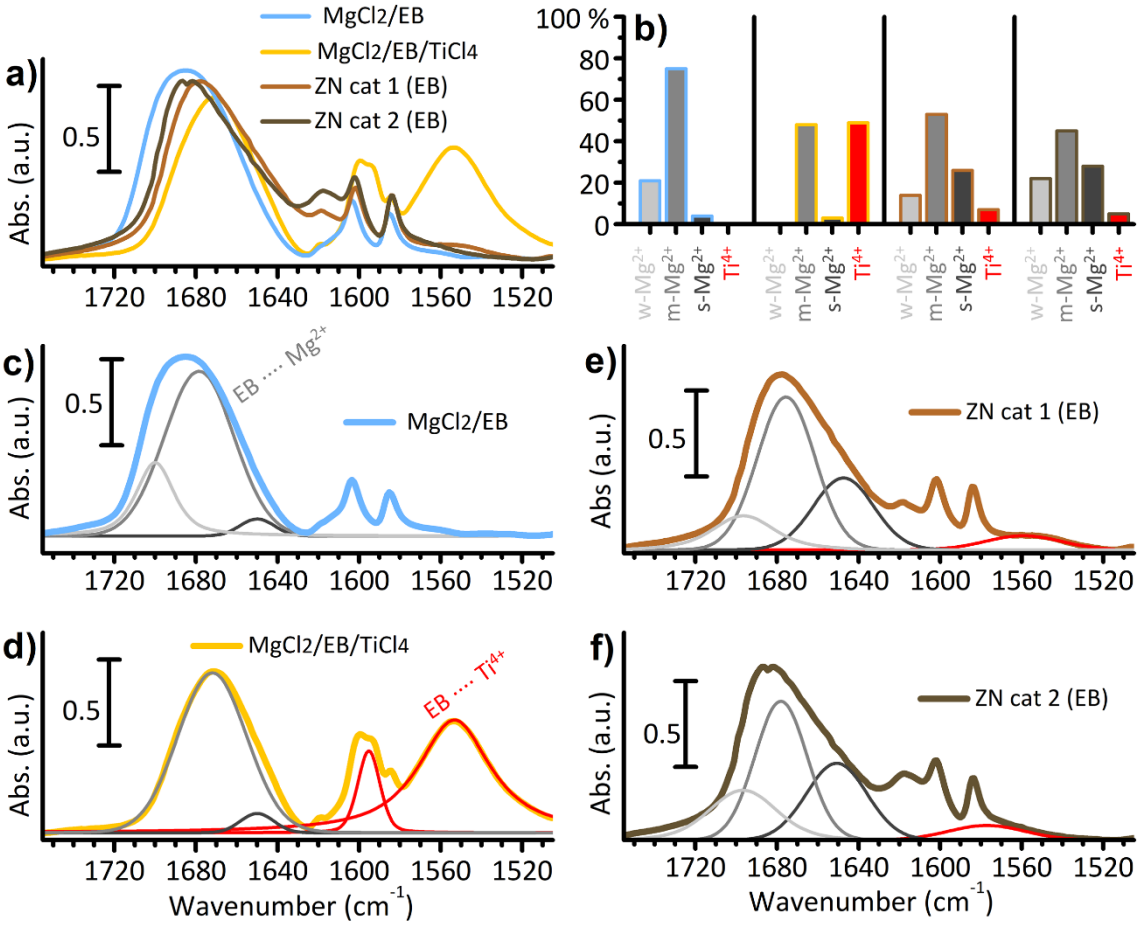

Figure 3. Part a) IR spectra in the 1800-1500 cm^{-1} range of $MgCl_2$/EB and $MgCl_2$/EB/$TiCl_4$ model systems [90], and of two EB containing industrial ZN catalysts, where $MgCl_2$ is obtained directly in the presence of $TiCl_4$, by either direct precipitation from alcohol solution (ZN cat 1) [91] or by conversion of a $Mg(OEt)_2$ precursor (ZN cat 2) [92]. Part b) Results of the curve fitting of the four IR spectra shown in part a, considering the contribution of EB adsorbed on weak, medium and strong acid Mg^{2+} sites (w-Mg^{2+}, m-Mg^{2+} and s-Mg^{2+}, respectively), and on Ti^{4+} sites, as determined in ref. [90]. The histograms reports the integrated areas of the four ν(C=O) contributions. Parts c-f) The same spectra as in part a together with the fitted bands corresponding to the four main contributions (with the same color code as in part b).

As an example of the potential of IR spectroscopy, Figure 3a shows the IR spectra of two models and two industrial ZN pre-catalysts containing ethylbenzoate (EB) as internal donor. The spectra are shown in the 1770-1510 cm^{-1} region, where ν(C=O) vibrational modes contribute to

the spectrum, together with two vibrational modes of the phenyl ring (weak but sharp bands at 1604 and 1585 cm^{-1}) [93]. The four spectra are clearly different, suggesting that the coordination mode of EB depends on the synthesis protocol. The spectrum of $MgCl_2$/EB (Figure 3c), a binary system obtained by adsorbing EB on a δ-$MgCl_2$ [90], is characterized by a broad and intense absorption band centered at 1690 cm^{-1}, which can be adequately fitted with three bands at 1700, 1675 and 1650 cm^{-1}, indicative for EB coordinated to weak, medium and strong acid Mg^{2+} cations, respectively [85, 90]. The integrated areas of those three bands can be used to estimate the relative abundance of the corresponding surface sites, as reported in Figure 3b. After addition of $TiCl_4$ from the vapor phase ($MgCl_2$/EB/$TiCl_4$, Figure 3d), the relative contribution of these three bands drastically changes. Especially the component at 1700 cm^{-1} is completely eroded, and a new broad absorption band appears in the 1590-1550 cm^{-1} range. The latter band is attributed to ν(C=O) of EB in interaction with Ti^{4+} [94], and is indicative of the formation of $TiCl_4$-EB complexes. The dip at 1580 cm^{-1} is originated by a Fermi resonance effect between the phenyl vibrational mode and the ν(C=O) falling at the same frequency [95, 96]. Therefore, the comparison of the spectra of $MgCl_2$/EB and $MgCl_2$/EB/$TiCl_4$ reveals that EB has a dynamic behavior in the presence of $TiCl_4$, as predicted by DFT calculations [97, 98]. In particular, half of the total EB migrates from the $MgCl_2$ surface to chemisorbed $TiCl_x$ species (Figure 3b). This phenomenon was further proved by IR spectroscopy of CO adsorbed at 100 K (-175 °C), which revealed an increase in the number of accessible Mg^{2+} sites upon addition of $TiCl_4$ on the $MgCl_2$/EB binary sample [90]. Such a result was rather counterintuitive, considering that $TiCl_4$ itself is known to occupy $MgCl_2$ surface [67], and it was explained by invoking the release of some Mg^{2+} sites previously occupied by EB molecules.

Very recently Liang et al. observed an analogous dynamic behavior also for tetrahydrofuran THF, on a $MgCl_2$/THF-based ZN catalyst for ethylene polymerization [99]. IR spectroscopy of CO adsorbed at -150 °C revealed an increase in the fraction of accessible Mg^{2+} sites at the $MgCl_2$ surface after $TiCl_4$ addition, which was ascribed to the partial desorption of THF from the $MgCl_2$ surface. However, quantitative analysis pointed out that only a minor fraction of THF is actually washed away during the catalyst synthesis (from 50 to 40 wt%). At the same time, the migration of THF through the surface to form $TiCl_4$-THF complexes was assessed by IR spectroscopy and by O 1*s* XPS analysis [100].

The results discussed so far for model systems are valid also for industrial catalysts. Figure 3e and Figure 3f show the IR spectra of two ZN pre-catalysts synthetized by reacting $TiCl_4$ at 100 °C either with a solution of $MgCl_2$ dissolved in alcohol (ZN cat 1) or with $Mg(OEt)_2$ (ZN cat 2), in both

cases in the presence of EB in the reaction mixture. The two spectra have been deconvolved in the same way as $MgCl_2$/EB and $MgCl_2$/EB/$TiCl_4$ model systems, resulting into four main contributions. In the range between 1630 and 1720 cm^{-1}, three main contributions correspond to EB coordinated to Mg^{2+} sites with different acid strength, as already described for the model samples, but in different proportion. As summarized in Figure 3b, in industrial ZN pre-catalysts EB probes many more defects at $MgCl_2$ surface. Moreover, a non-negligible amount of $TiCl_4$-EB complexes (about 7 and 5 % of the total, respectively) is also visible in both cases (band at about 1560 cm^{-1}), despite the repeated washing steps during the synthesis.

Figure 4 shows the IR spectrum of a ZN pre-catalyst synthetized with the same protocol as ZN cat 2(EB) but using dibutylphthalate (DBP) as internal donor, which is still one of the most commonly used in industrial practice [47, 101]. The introduction of DBP marked the beginning of the fourth generation of ZN catalysts in early 80's [3, 102], although in the last years REACH restrictions have been fostering the development of new phthalates-free ZN catalysts [47]. Also in this case the ν(C=O) band can be deconvolved with three main components at 1657, 1680 and 1707 cm^{-1}, whose assignment however is more complicate than for EB, because of the many possible configurations of DBP at each adsorption site (monodentate, chelate or bridged) [85, 87, 89, 103]. The fit is completed by two additional bands at 1758 and 1634 cm^{-1}, respectively. The former is assigned to ν(C=O) of phthaloyl chloride (POC) [84], which originates from a side reaction of some DBP molecules with $TiCl_4$ [104], and accounts for about 12 % of the total (Figure 4b). The formation of POC in certain experimental conditions was reported previously, and is generally correlated to worst catalytic performances [105]. The band at 1634 cm^{-1}, instead, is due to DBP in bonding interaction with Ti^{4+} [106], and provides evidence on that a few DBP molecules are directly coordinated to the Ti sites. The DBP in complexes with $TiCl_x$ species accounts for about 6 % of the total (Figure 4b). Such analysis is in fine agreement with the ^{1}H and ^{13}C NMR spectroscopic characterization performed by Gupta and coworkers on analogous catalysts [105].

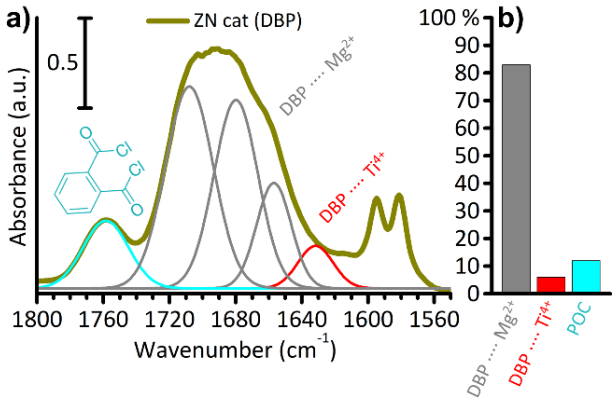

Figure 4. Part a) IR spectrum of a DBP containing industrial-like ZN catalyst, obtained by direct reaction of $TiCl_4$ with $Mg(OEt)_2$ precursor in the presence of DBP [92, 107, 108]. The five main ν(C=O) contributions necessary to reproduce the experimental spectrum are also reported (in grey those corresponding to DBP in interaction with Mg^{2+}, in red that with Ti^{4+}, and in light blue that corresponding to POC). The same analysis has been lately applied to investigate the evolution of the components upon the synthesis of an analogous ZN catalyst [109]. Part b) Result of the curve fitting, in terms of integrated areas of the ν(C=O) bands. Note that in this case it is not possible to discriminate between DBP adsorbed on Mg^{2+} sites with different acidity, due to the multiple configurations possible for DBP.

The IR spectroscopic data summarized in this section clearly demonstrate three main facts. 1) The internal donors play a fundamental role as capping agents for disordered δ-$MgCl_2$ nanoparticles [50, 110, 111], stabilizing under-coordinated (and strongly acidic) Mg^{2+} sites by chemisorption [112] and thus lowering the surface energy of otherwise not favored surfaces and defects [69, 113]. This is in agreement with other reports in the literature. 2) The internal electron donors have a certain dynamic behavior and can move at the catalyst surface depending on the experimental conditions, thus indicating that they are not so tightly bonded at the adsorption sites. 3) Last, but not least, Ti^{4+}-donor complexes have been observed not only on the two model systems, but also on the industrial pre-catalysts in ZN pre-catalysts, even after several washing steps. Nevertheless, the effective participation of internal donors in the catalytic sites after reaction with the Al-alkyl activator is still a controversial point, since a certain clean-up is known to take place, as demonstrated for the first time with GC-MS analysis in 1982 [114]. According to recent quantitative investigation by Busico and coworkers, the molar percentage of Ti and of the donor molecules after the activation are comparable when the reaction is carried out at 40 °C, but at higher temperatures the donor amount drops down, while the amount of Ti remains almost constant up to 100 °C [115, 116]. Therefore, the persistence of the donors in the Ti coordination sphere under working conditions appears to be temperature-dependent.

Finally, it is worth remembering that electron donors may not be the only externals additives around the Ti centers: the by-products of ZN pre-catalyst activation by Al-alkyl molecules likely stay adsorbed on the catalyst surface in close proximity of the metal sites, thus behaving as additional ligands themselves. However, that occurrence is hardly detectable by IR spectroscopy because the fingerprints of those by-products are intrinsically weakly intense and scarcely sensitive to interactions with the surroundings. Other characterization techniques may hence come in handy, as the magnetic spectroscopies briefly outlined in Section 3.

2.1.2. The products of chromates reduction in industrial Phillips catalyst: unexpected weakly coordinated ligands

The Phillips catalyst is apparently much simpler in composition than ZN catalysts, so that it has been often regarded as an example of single-site catalyst. In its basic formulation, the pre-catalyst can be described in terms of highly diluted mono-chromates covalently grafted at the surface of an amorphous silica, without any additional component acting as weakly coordinated ligand. In industrial practice the pre-catalyst is activated by the ethylene monomer itself at 80-110 °C during a certain induction time, necessary for reducing and alkylating the Cr species [117]. In this process, two formaldehyde molecules are produced per Cr site as by-products from oxidation of ethylene, as detected in a few cases by mass spectrometry (MS) analysis [117-119]. For long time formaldehyde was thought to be easily removed from the catalyst at the polymerization temperature, either as such or as a CO_2/H_2O mixture after a theoretically affordable second reaction with another chromate [120]. However, recent temperature-programmed desorption (TPD) experiments carried out on ethylene-activated Phillips catalysts revealed that some oxygenated compounds remain adsorbed at the catalyst surface [121, 122]. In particular, during the TPD run, CO_2 (m/z = 44) evolution was observed above 200 °C, together with a signal at a m/z of 15 (i.e., a methyl group), suggesting the presence on the catalyst of two-carbons species easily decomposing into CH_4 and CO_2, e.g. acetate or methylformate compounds, or two separate one-carbon ligands on the same Cr site [122]. It has been hypothesized that such species derive from a rearrangement of the two formaldehyde molecules produced at the same Cr site. The sole analysis of the TPD outputs cannot discriminate among these possible species neither assess whether they are adsorbed at the Cr sites (hence acting as weakly bonded ligands) or simply at the silica surface.

IR spectroscopy has the potential to answer to these questions, since the vibrational modes of the possible oxygenates deriving from oxidation of ethylene are strongly IR active and sensitive

to the adsorption site. Therefore, the fate of formaldehyde was studied by IR spectroscopy, monitoring in situ the evolution of the spectra during the reaction of ethylene with the Phillips catalyst in mild conditions (P_{C2H4} = 100 mbar, T = 150 °C). A few relevant spectra are shown in Figure 5a). The spectrum of the starting Cr(VI)/SiO_2 pre-catalyst (spectrum 1) recopies that of a highly dehydroxylated silica, with a sharp band at 3750 cm^{-1} ascribed to ν(OH) of isolated surface silanols, and off-scale signals below 1300 cm^{-1} due to the vibrational modes of silica bulk, whose overtones give well defined bands at 1640, 1865 and 1970 cm^{-1}. The spectrum collected after a few minutes of reaction with ethylene (spectrum 2) displays, beside the fingerprints of gaseous ethylene (well-distinguishable roto-vibrational profile above 3000 cm^{-1}), an intense band at 1570 cm^{-1} with a broad tail at about 1617 cm^{-1} (magnified in the inset). These two bands further grow in intensity after 30 minutes of reaction (spectrum 3), simultaneously to the appearance of the ν(CH_2) bands characteristic of polyethylene at 2980 and 2820 cm^{-1} [123, 124], which demonstrate the occurrence of ethylene polymerization. The two bands around 1600 cm^{-1} have been straightforwardly assigned to vibrations involving oxygenated species, and in particular to the ν(C=O) mode of methylformate adsorbed on reduced Cr sites, whose formation is fostered by the Cr sites themselves, acting as Lewis acids [125, 126].

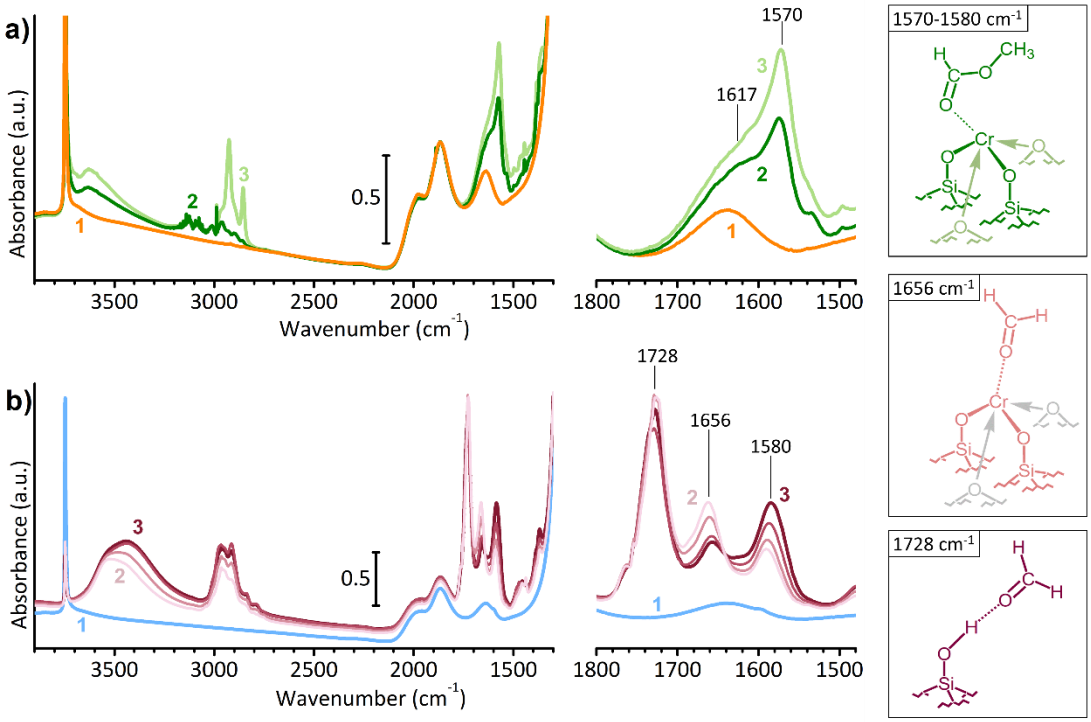

Figure 5. Part a) IR spectrum of Cr(VI)/SiO_2 Phillips catalyst (spectrum 1) and its evolution in time in the presence of ethylene at 150 °C (spectrum 2 after 30 min, spectrum 3 after 60 min) [125]. Part b) IR spectrum of CO-reduced Cr(II)/SiO_2 Phillips catalyst (spectrum 4) and its evolution in time in the presence of formaldehyde (from spectrum 5 to

6); the same experiment is reported as supporting material in ref. [125]. Insets on the right side show a magnification of the 1800-1500 cm^{-1} range, together with the sketch of the species mainly contributing in that range.

As a proof of concept, Figure 5b shows the FT-IR spectra of a CO-reduced Phillips catalyst, Cr(II)/SiO_2 (spectrum 1), in interaction with formaldehyde in the vapor phase. The spectra are shown as a function of the contact time for about 20 minutes [125]. Reduction in CO at 350 °C is known to stoichiometrically reduce the mono-chromates into "naked" Cr(II) species, i.e. highly uncoordinated Cr(II) sites covalently bonded to silica through two O atoms [127-131]. As soon as formaldehyde is adsorbed on Cr(II)/SiO_2 (spectrum 2), three intense absorption bands are observed in the ν(C=O) stretching region (1800 – 1550 cm^{-1}), which evolve differently with time and correspond to formaldehyde adsorbed on different sites. The band at 1728 cm^{-1} (i.e., slightly red-shifted with respect to pure formaldehyde) is attributed to formaldehyde in interaction with the silanol groups at silica surface and does not evolve with time. In contrast, the band at 1656 cm^{-1}, ascribed to formaldehyde adsorbed on strongly acidic Cr(II) sites, rapidly decreases in intensity in favor of a new one at 1580 cm^{-1} (as magnified in the inset). The isosbestic point at 1642 cm^{-1} provides compelling evidence that the new species is formed at the expenses of the former one. This sequence of spectra has been explained as the disproportionation of two formaldehyde molecules into a single methylformate molecule through a Cr(II)-promoted Tishchenko reaction [132-135]. The similarity of spectra 3 in Figure 5a and Figure 5b is particular striking and allows to conclude that the oxygenated by-products formed upon reduction of Cr(VI)/SiO_2 by ethylene are coordinated to the reduced Cr species.

It is worth noticing that methylformate on the Phillips catalyst is produced also when Cr(VI)/SiO_2 is photo-reduced by ethylene under UV-Vis irradiation at room temperature [136]. In that case, however, ethylene oxide is detected as well, likely as a consequence of a specific photoactivation mechanism involving the reaction of one single oxygen atom at a time for each mono-chromate species [137-140].

The IR data discussed above provide unequivocal evidence on the nature of the oxygenated by-products formed when Cr(VI)/SiO_2 is reduced in ethylene, which were only indirectly hypothesized on the basis of the species detected in the reactor by MS analysis at the end of the industrial polymerization process [121, 122], but never directly observed. Even more important, IR spectroscopy proves that these by-products remain in the coordination sphere of the reduced Cr species, and hence must be considered as ligands (L') taking part to the definition of the active sites. In this respect it is worth remarking that, even though the CO-reduced Cr(II)/SiO_2 catalyst has

been considered for long time as representative for the industrial (ethylene-reduced) Phillips catalyst at the end of the induction time [6, 127, 129] and thus used to investigate the initiation mechanism in ethylene polymerization and the structure of the propagating Cr species [141-144], nevertheless the reduced Cr(II) sites obtained upon reduction of mono-chromates in CO are missing the oxygenated by-product nearby. Indeed, pre-reduction in CO produces CO_2 as a by-product, which is easily desorbed from the catalyst surface.

The presence or absence of the oxygenated by-products in the Cr coordination sphere has important consequences on their electronic properties, as revealed by UV-Vis spectroscopy [125]. Figure 6 compares the DR UV-Vis spectrum of the CO-reduced Cr(II)/SiO_2 catalyst (spectrum 1) with those of Cr(VI)/SiO_2 reduced in ethylene, either thermally (spectrum 2) or under UV irradiation (spectrum 3), before the onset of the polymerization reaction. The spectrum of Cr(II)/SiO_2 displays three characteristic bands centered at 30000, 12000 and 7000 cm^{-1}: the former is ascribed to an O(2*p*)→Cr(3*d*) charge-transfer transition, while the latter two are assigned to d-d transitions. The whole spectrum is regarded as the fingerprint of highly uncoordinated Cr(II) sites [145, 146]. It has been widely demonstrated that all the three bands are very sensitive to a change in the coordination of the Cr(II) sites: adsorption of molecules generally causes an upward shift of both the d-d bands and a decrease in intensity of the CT band, as theoretically predicted by the ligand-field theory [147]. The spectra of the two ethylene-reduced Cr/SiO_2 samples are pretty similar to each other: the CT and d-d bands are upward shifted with respect to the CO-reduced Cr(II)/SiO_2 sample, providing a compelling evidence that the majority of Cr(VI) sites have been reduced by ethylene to Cr(II) and that the oxygenated by-products remain in the Cr(II) coordination sphere.

The subtle difference among samples reduced in CO or in ethylene has an effect on the catalytic performances. Indeed, it has been reported that the CO-reduced Phillips catalyst produces a polyethylene with a lower density, due to a higher in situ branching and a favored chain termination [6, 148]. Interestingly, the adsorption of acetic acid prior to ethylene dosage onto a Phillips catalyst pre-reduced in CO leads to the production of a polyethylene much more similar to the one produced in the industrial process by the ethylene-activated catalyst [126].

The combination of the spectroscopic observations with the catalytic data reiterates once again that, irrespective to the common Cr oxidation state, the presence of weakly coordinated ligands do make the difference in ethylene polymerization catalysis and thus must be carefully taken into account [125, 126].

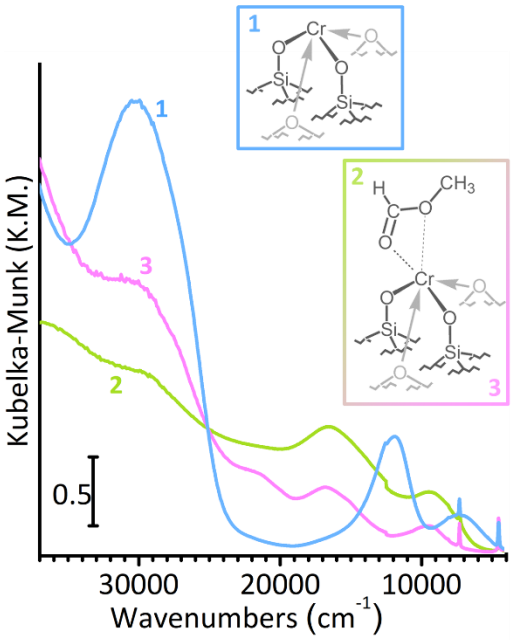

Figure 6. DR UV-Vis spectra of three Cr(II)/SiO_2 catalysts obtained from Cr(VI)/SiO_2 by different reduction treatments: in CO at 350 °C (spectrum 1), in ethylene at 150 °C (spectrum 2) or in ethylene at room temperature under UV irradiation (spectrum 3). In the latter two cases, the spectra are collected when the majority of Cr(VI) sites have been reduced but before the onset of the ethylene polymerization reaction. The differences with respect to spectrum 1 are due to the presence of the by-products of ethylene oxidation in the Cr(II) coordination sphere, as schematically depicted in the sketches.

2.2. The support material as a macro-ligand

2.2.1. The influence of the $MgCl_2$ support on the properties of the Ti sites in Ziegler-Natta catalysts

In the field of ZN catalysis, it has been widely demonstrated that the method of preparation of activated $MgCl_2$ affects the overall catalytic activity [149]. This in turn suggests that $MgCl_2$ itself affects the distribution of the Ti sites, before any other influence exerted by the electron donors. Nevertheless, while the role of electron donors has been the object of many investigations, the effect of the $MgCl_2$ support has been rarely discussed. In part, this is due to the fact that the majority of industrial ZN pre-catalysts are obtained through a one-pot synthetic strategy, whereby the Mg precursor, $TiCl_4$ and the donor are added simultaneously or consecutively in the same reaction pot. Hence, it becomes difficult to analyze separately the effect of the internal donors and that of the $MgCl_2$ support on the properties of the $TiCl_x$ species. This is possible, however, on model ZN pre-catalysts synthetized in the absence of any internal donors. In this section we will

demonstrate that DR UV-Vis spectroscopy is able to detect subtle differences in the electronic properties of the Ti sites depending on the type of $MgCl_2$ support.

Figure 7 displays the diffuse reflectance (DR) UV-Vis spectra of two model ZN pre-catalysts obtained by reacting $TiCl_4$ vapors at 90 °C with two different $MgCl_2$ supports, namely a dry ball-milled $MgCl_2$ ($MgCl_2$(1), with a specific surface area SSA of 73 m^2/g) [111] and a $MgCl_2$ obtained through a controlled dealcoholation of a $MgCl_2$-$6CH_3OH$ adduct in N_2 flux at 250 °C ($MgCl_2$(2), with a SSA of 100 m^2/g) [150]. The amount of Ti in both cases is about 1 wt%, respectively. In both spectra, all the absorption bands are exclusively due to the grafted $TiCl_x$ species, with no interactions other than with the $MgCl_2$ support.

Generally speaking, the observed bands are all due to Cl(2*p*)→Ti(3*d*) ligand-to-metal charge transfer (CT) transitions; the analysis of these bands has been thoroughly discussed in our last work, providing the interpretation key for all the UV-Vis spectra of analogous $MgCl_2$-supported ZN pre-catalysts [151]. More in details, the spectrum of $MgCl_2$(1)/$TiCl_4$ shows two well-defined bands at 33600 and 40000 cm^{-1} (the former with a shoulder at 29950 cm^{-1}), which are ascribed to Cl(2*p*)→Ti(3*d*t_{2g}) and Cl(2*p*)→Ti(3*d*e_g) transitions, respectively, in the approximation of pseudo-octahedral coordination. Cl(2*p*)→Ti(3*d*t_{2g}) transition is split in two components due to the non-equivalence of the chlorine anions. The energy separation between the two bands allows to estimate the crystal field splitting of the Ti 3*d* orbitals (Δ_{CF}), which is a direct indication of the effective charge on the Ti sites. The spectrum of $MgCl_2$(2)/$TiCl_4$ shows broader bands, shifted at lower energy and with a larger Δ_{CF} value. This suggests a greater heterogeneity of the grafted Ti sites in $MgCl_2$(2)/$TiCl_4$, which are, in average, more positive than in $MgCl_2$(1)/$TiCl_4$. Indeed, a lower electron density at the Ti^{4+} sites facilitates the electron transfer from the Cl ligands, explaining both the shift of the bands at lower energy and the larger Δ_{CF} value.

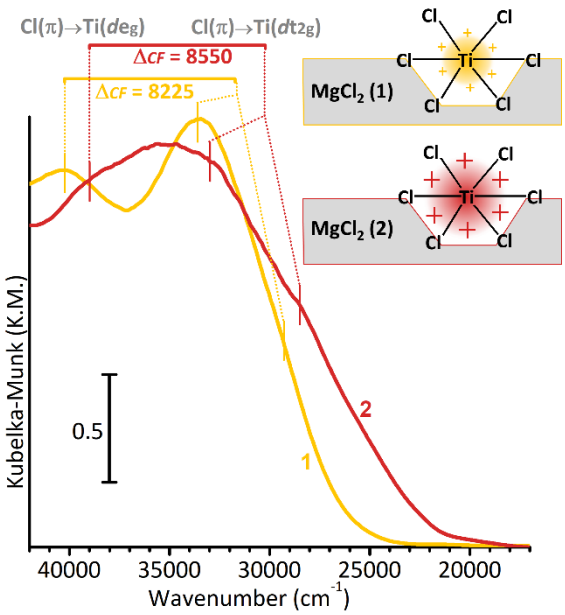

Figure 7. DR UV-Vis spectra of two different $MgCl_2/TiCl_4$ samples, obtained by reaction of $TiCl_4$ vapors at 90 °C with either dry ball-milled $MgCl_2$ (1) [111], or with the $MgCl_2$ formed upon dealcoholation at 250 °C of a $MgCl_2$-$6CH_3OH$ adduct (2) [150]. The two sketches represent the active sites in the two samples, characterized by the same local structure but different positive charge on the Ti ion.

These data demonstrate the potential of UV-Vis spectroscopy in highlighting the effect of the $MgCl_2$ support on the electronic properties of the Ti^{4+} sites in ZN pre-catalysts. According to recent theoretical calculations, the effective charge on the Ti sites in the pre-catalysts correlates with the activation energy for olefin insertion in the Ti-alkyl bond of the corresponding activated catalysts [152, 153], and hence with the overall activity of the catalytic process. Hence, controlling the surface properties of $MgCl_2$ support and its interaction with the grafted Ti species is of paramount importance.

2.2.2. The flexibility of Cr sites at the surface of amorphous silica support in the Phillips catalyst

Despite the apparent rigidity of metal oxides frameworks, amorphous silica is a quite flexible material, whose interaction with the supported metal sites strongly depends on the working parameters, such as the activation/reaction temperature and the chemical atmosphere. This phenomenon has been deeply studied for the Phillips catalyst, especially in its CO-reduced form. It has been already discussed in the previous section that reduction of the $Cr(VI)/SiO_2$ catalyst in CO at 350 °C leads to the stoichiometric conversion of all the mono-chromates into highly uncoordinated ("naked") Cr(II) sites. These Cr(II) species have a strong tendency to increase their coordination sphere through adsorption of small molecules. What has been not discussed yet is

that the adsorption of external ligands leads to a rearrangement of the Cr(II) sites at the silica surface, comprising the elongation of the Cr-O covalent bonds as well as the displacement of siloxane bridges weakly bonded nearby. That is to say that the Cr(II) sites are not rigidly fixed at the SiO_2 surface, but display a certain flexibility in response to external stimuli. Hence, the whole silica support behaves as the strongly coordinated ligands (L) in homogenous catalysis.

The most insightful experimental evidence of this surface flexibility comes from IR spectroscopy of adsorbed CO. Some representative IR spectra are reported in Figure 8a. Since the early 1960s, it was demonstrated that mono- and di-carbonyls are formed when CO is adsorbed at room temperature on $Cr(II)/SiO_2$, whose IR spectrum (spectrum 2 in Figure 8a) shows a characteristic triplet of bands at 2189, 2182 and 2176 cm^{-1} [131, 154-159]. These ν(C≡O) stretching frequencies reveal that the adsorption process is dominated by σ-donation effects, which is unlikely for homogeneous Cr complexes, and hence indicate that the silica surface provides uncommon opportunities for stabilizing the Cr(II) species. However, when CO is adsorbed on $Cr(II)/SiO_2$ at 100 K (i.e. at high CO coverage [160], spectrum 3 in Figure 8a) the IR spectrum drastically changes, displaying a multitude of bands below 2100 cm^{-1}, which are indicative of the formation of multi-carbonyls dominated by π-backdonation effects [155]. The drastic change of type of interaction between CO and the Cr(II) sites (from σ-donation to π-backdonation) unequivocally demonstrates that upon formation of multi-carbonyls the Cr(II) sites loose their tight interaction with the silica surface, behaving now very much like homogeneous Cr complexes. This is made possible by the flexibility of the silica surface: the addition of further CO molecules in the Cr(II) coordination sphere occurs at the expenses of weakly coordinated, hemi-labile, siloxane ligands. In other words, the Cr(II) sites are able to coordinate a multitude of external ligands by progressively displacing the hemilabile siloxane bridges belonging to the silica surface. The process is completely reversible by going back to room temperature [158].

The phenomenon discussed above is accompanied by an important rearrangement of the Cr(II) local structure, and in particular by the elongation of the covalent Cr-O bonds which link the Cr(II) sites at the silica surface. Cr K-edge EXAFS spectroscopy gives a direct measure of the distances of the atoms around the Cr sites. Figure 8b and Figure 8b' show the modulus and the imaginary part of the Fourier-Transformed k^3-weighted χ(k) functions for $Cr(II)/SiO_2$ (spectrum 1) and for the same sample measured in the presence of CO either at room temperature (spectrum 2) or at 100 K (spectrum 3). The spectrum of $Cr(II)/SiO_2$ is constituted by two main components peaked at 1.35 and 2.34 Å (not corrected in phase). According to the EXAFS fit, the former is due

to the contribution of two O atoms at 1.86 Å, while the latter to two Si atoms at about 2.70 Å. It is important to observe that weakly interacting siloxane bridges in the Cr(II) surroundings almost do not contribute to the EXAFS signal, because the large heterogeneity in distances is responsible for very high static Debye-Waller factors and cancellation effects for the imaginary parts of the Fourier Transformed χ(k) function. Upon CO adsorption, both components increase in intensity and shift at longer distances. The shift can be well appreciated by looking to the imaginary parts of the χ(k) function. The increase in intensity is due not only to the increase in the number of ligands, but also to a decrease of the overall Debye-Waller factor: indeed, both the dynamic and static components of the Debye-Waller are smaller than for Cr(II)/SiO_2, the former because of temperature effect, and the latter because the formation of multi-carbonyls attenuates the heterogeneity of sites. The EXAFS fit indicates that, on average, 2.5 CO molecules are adsorbed per Cr(II) sites. More interestingly, the formation of multi-carbonyls makes Cr(II) sites emerging from the surface, with a consistent elongation of the Cr–O distance of 0.075 Å, from 1.86 to 1.935 Å [161], as schematically shown in Figure 8e (left).

The elongation of the covalent Cr–O bond upon CO adsorption is reflected in the vibrational spectrum of Cr(II)/SiO_2. Figure 8c shows the Raman spectra of Cr(II)/SiO_2 before (spectrum 1) and after CO adsorption at room temperature (spectrum 2). In order to exploit the selective resonant intensification and to bring out the signals of Cr(II) species from the absorptions of silica framework, the two spectra have been respectively collected exciting the sample with a 442 nm (= 22625 cm^{-1}) blue laser when in vacuum, and with a 325 nm (= 30770 cm^{-1}) violet laser when in the presence of CO [162]. Two Raman active vibrational modes characteristic of CO-reduced (≡SiO)$_2$Cr(II) species are clearly observed at 1009 and 568 cm^{-1}, which shift in position upon coordination of CO, respectively at 1048 and 542 cm^{-1}. Both bands occur in the spectral region characteristic for the vibrations of the silica support: hence, they have been interpreted as due to silica framework modes perturbed by the presence of the Cr(II) cations, emerging from the background because of the resonant intensification effect [162]. It is worth noticing that the latter can also be due to the fundamental ν(Cr–O) mode, whose position and extinction coefficient strongly depends on the length and on the electric dipole of the bond [163]. The shift of both bands upon CO adsorption is a direct proof of a change in the local structure of the Cr(II) species.

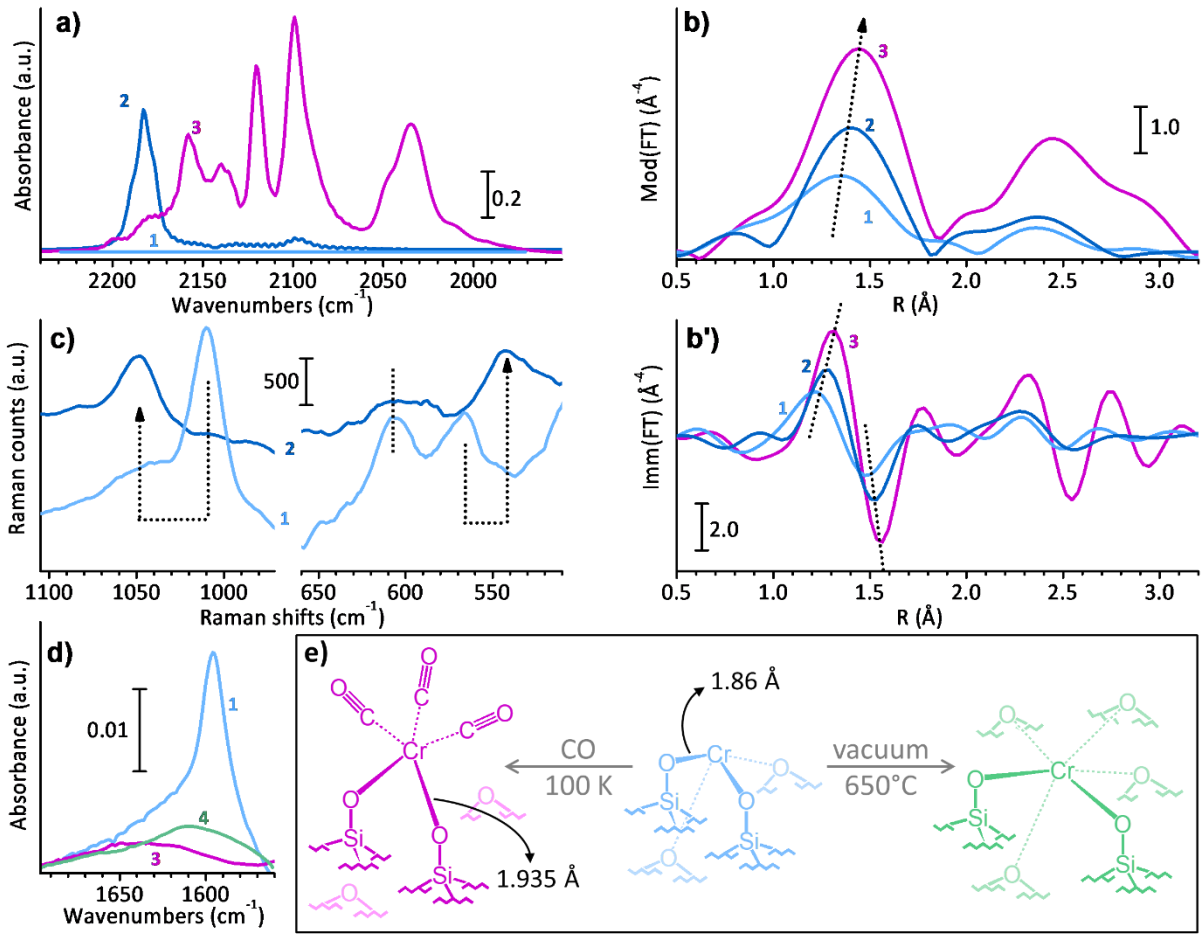

Figure 8. Part a) FT-IR spectra in the ν(CO) region, of Cr(II)/SiO_2 (spectrum 1) and of the same sample measured in the presence of CO either at room temperature (spectrum 2) or at 100 K (spectrum 3) [158]. The spectra are shown after subtraction of that of Cr(II)/SiO_2. Parts b and b'): modulus and imaginary part of the Fourier-Transformed k^3-weighted χ(k) functions for Cr(II)/SiO_2 (spectrum 1) and for the same sample measured in the presence of CO either at room temperature (spectrum 2) or at 100 K (spectrum 3) [161]. Part c) Raman spectra of Cr(II)/SiO_2 and of the same sample measured in the presence of CO at room temperature, collected respectively with a 442 nm and a 325 nm laser excitation to exploit the resonance effect [162]. The dotted lines are visual guides to highlight the spectral changes in the presence of CO. Part d) FT-IR spectra of Cr(II)/SiO_2 (spectrum 1) and of the same sample measured in the presence of CO at 100 K (spectrum 3), or after a thermal treatment at 650 °C (spectrum 4). The spectra are shown after subtraction of that of pure silica treated at the same temperature. Part e) schematic representation of the dynamic behavior of Cr(II) sites at SiO_2 surface either in presence of CO (left) or as a consequence of thermal treatment at high temperature (right). In both cases, an elongation of the Cr-O covalent bonds has been detected by spectroscopy. The bond lengths reported on the left side were determined by EXAFS.

A similar information can be obtained by IR spectroscopy, even though much less evident because it is not possible to exploit the resonance effect. Figure 8d shows the IR spectra of Cr(II)/SiO_2 in vacuum (spectrum 1) and in the presence of CO at low temperature (spectrum 3) in the 1700 – 1550 cm^{-1} region, after subtraction of the spectrum of pure silica treated at the same

temperature. A weak but sharp band is observed at 1596 cm^{-1} in the spectrum of Cr(II)/SiO_2, which closely resembles the band at 1048 cm^{-1} observed in the Raman spectrum in Figure 8c. Even though the assignment of this band is not straightforward, we tentatively ascribe it to the combination of two silica framework modes detected by Raman, one perturbed by the presence of the Cr(II) sites (1048 cm^{-1}) and the other not (606 cm^{-1}, whose variation in intensity is just due to the different laser used for the excitation). Whatever the origin of the band at 1596 cm^{-1}, it is unequivocally sensitive to CO adsorption: in spectrum 3, it decreases in intensity and shifts at higher wavenumbers, very much like to what happens to the 1048 cm^{-1} band in the Raman spectra. The phenomenon is reversible upon decreasing the CO pressure.

All in all, the spectroscopic data summarized in Figure 8 unequivocally demonstrate that the Cr(II) sites have a flexible behavior at the silica surface, assisted by the hemilabile nature of the weakly coordinated siloxane ligands. Adsorption of external ligands causes a rearrangement of the Cr(II) sites, with an average elongation of the Cr-O covalent bond and a gradual loss of the weak interaction with the support (Figure 8e, left).

But that is not the whole story. As anticipated at the beginning of the section, Cr(II) species in the CO-reduced Cr(II)/SiO_2 system do not respond only to the presence of external ligands, but they also manifest a flexible behavior when treated at high temperature [158]. A first important proof of this phenomenon comes once again from DR UV-Vis spectroscopy. The UV-Vis spectra of Cr(II)/SiO_2 systems reduced in CO at increasing temperatures (350, 400 and 500 °C) show a progressive abatement in intensity of the CT band at about 30000 cm^{-1} [164], which provides a compelling evidence that the treatment at high temperature induces the formation of Cr(II) sites more coordinated than those obtained at lower temperature. The same behavior has been observed upon annealing a standard Cr(II)/SiO_2 system at high temperature in vacuum: also in that case, the UV-Vis spectra indicate an increase in the number of ligands in the Cr(II) coordination sphere [158]. Both experiments indicate that the Cr(II) sites have the tendency to sink in the silica framework upon treatment at high temperature, with the consequence that they are less available for incoming molecules, including ethylene [158]. Indeed, annealed Cr(II)/SiO_2 adsorbs much less CO than standard Cr(II)/SiO_2, and shows a reduced ability in ethylene polymerization [158]. Interestingly, IR spectroscopy indicates that the sinking of the Cr(II) sites in the silica framework upon annealing occurs through elongation of the average Cr-O bonds (as schematically suggested in Figure 8e, right). Indeed, the IR spectrum of the annealed Cr(II)/SiO_2 system in the 1700 – 1550

cm^{-1} region (spectrum 4 in Figure 8d) shows a drastic abatement in intensity of the band at 1596 cm^{-1}, characteristic for highly uncoordinated Cr(II) sites.

3. CONCLUSIONS

The selection of spectroscopic results presented in this work offers a unique point of view on the two main families of heterogeneous catalysts for olefin polymerization, demonstrating that, despite the solid state, they are anything but rigidly fixed. In this respect, the principles of coordination chemistry (typical for homogeneous catalysts) should be taken into account as guidelines for the description of the catalytic active sites (while keeping in mind the limitations arising from the heterogeneity of the sites and the coexistence of both active and inactive species). As a matter of fact, in both ZN and Phillips catalysts the active phase is constituted by isolated transition metal species, strongly coordinated from one side by the support material (whose surface properties can be controlled during the synthesis or by post-synthesis treatments), and from the other side weakly interacting with organic molecules, either externally added on purpose during the preparation of the catalysts (as the electron donors in the case of ZN) or spontaneously generated during the catalytic process (as the by-products of ethylene oxidation in the case of Phillips). From both sides, those components behave as flexible and dynamic ligands around the active sites, very much sensitive to external chemical and thermal stimuli, shortening or elongating the bond length, assuming different dispositions and conformations, and modulating the steric hindrance around the metal sites and its electron density.

It is important to notice that optical spectroscopies are not the only characterization techniques able to selectively detect the fingerprints of specific interactions and quantitatively evaluate their strength. Indeed, also magnetic spectroscopies can fulfill this demand, thanks to their extreme sensitivity to precise isotopes and/or oxidation states and to their high tunability through the modulation of the magnetic field and the application of specific pulse sequences. For instance, ^{13}C NMR spectroscopy has been extensively used to investigate the influence of electron donors in ZN pre-catalysts [165-167], very recently enhancing the resolution on the structural details of the surface sites by transferring the larger polarization of free radicals in the solvent to targeted NMR active nuclei via classical cross-polarization approach (the so called dynamic nuclear polarization surface-enhanced NMR spectroscopy, DNP-SENS) [168, 169]. Upon activation of ZN catalysts, the reduction of the Ti centers to the paramagnetic +3 oxidation state makes NMR measures terribly difficult, but it opens the possibility to probe the interactions of the Ti sites with

the surroundings by use of advanced EPR spectroscopy: 2-D HYSCORE experiments have been performed to directly measure the hyperfine interaction of Ti^{3+} with ^{27}Al nuclei from the activator [170-173]. On the other hand, in the case of Phillips catalysts the use of magnetic spectroscopies have been so far much more limited, with a few EPR measures devoted to unravel which is the Cr oxidation state actually involved in ethylene polymerization [144, 174], and only one remarkable example of ^{29}Si NMR spectroscopy for monitoring the interaction between Cr species and SiO_2 support depending on the working conditions [175]. Further technical developments are thus needed to gain more details on the ligands around the Cr sites.

Even though the discussion contained in this review does not cover the whole complexity of heterogeneous catalysts for olefin polymerization, we hope it will inspire the work of other researchers in the field, fostering the awareness on the delicate equilibria governing the catalysis, which must be taken into account in the design and optimization of the process.

ACKNOWLEDGMENTS

The study and research work of the Authors in the field of olefin polymerization catalysis in the last years was made possible by two main financial supports: project “Cr4FUN - Chromium catalysis: from fundamental understanding to functional aliphatic polymers” funded by MIUR within the frame PRIN 2017 (20179FKR77_002), and project "DisMgCl - Structure determination at the nanoscale and atomic dynamics of MgCl2 primary particles in Ziegler-Natta catalysts" funded by DPI (#802).

REFERENCES

[1] T.E. Nowlin, Business and Technology of the Global Polyethylene Industry, Wiley-Scrivener, New York, 2014.
[2] J. Jansz, Global PO&E News Analysis, Chemical Market Resources, Inc., 2015.
[3] P. Galli, G. Vecellio, Technology: driving force behind innovation and growth of polyolefins, Prog. Polym. Sci., 26 (2001) 1287-1336.
[4] P.S. Chum, K.W. Swogger, Olefin polymer technologies—History and recent progress at The Dow Chemical Company, Prog. Polym. Sci., 33 (2008) 797-819.
[5] V. Busico, Catalytic Olefin Polymerization is a Mature Field. Isn't it?, Macromol. Chem. Phys., 208 (2007) 26-29.
[6] M.P. McDaniel, A Review of the Phillips Supported Chromium Catalyst and Its Commercial Use for Ethylene Polymerization, Adv. Catal., 53 (2010) 123-606.
[7] Polyolefins Market Share, Size, Trends, Industry Analysis Report By Feedstock (Polyethylene, Polypropylene, Ethylene Vinyl Acetate, Thermoplastic Olefins, Others), By Application (Film & Sheet, Injection Molding, Blow Molding, Extrusion Coating, Fiber, Others), By Regions, Segments & Forecast, 2019 - 2026, Polaris Market Research, 2019.

[8] P. Cossee, Ziegler-Natta catalysis I. Mechanism of polymerization of α-olefins with Ziegler-Natta catalysts, J. Catal., 3 (1964) 80-88.
[9] V. Busico, Giulio Natta and the Development of Stereoselective Propene Polymerization, in: W. Kaminsky (Ed.) Polyolefins: 50 years after Ziegler and Natta I, Springer, Berlin, 2013, pp. 37-57.
[10] T.Q. Nguyen, H.H. Kausch, Molecular Weight Distribution and Mechanical Properties, in: G.M. Swallowe (Ed.) Mechanical Properties and Testing of Polymers: An A-Z Reference, Springer Science, Dordrecht (Netherlands), 1999, pp. 143-150.
[11] C. Chen, Designing catalysts for olefin polymerization and copolymerization: beyond electronic and steric tuning, Nat. Rev. Chem., 2 (2018) 6-14.
[12] W. Keim, A. Behr, B. Gruber, B. Hoffmann, F.H. Kowaldt, U. Kuerschner, B. Limbaecker, F.P. Sistig, Reactions of chelate ylides with nickel(0) complexes, Organometallics, 5 (1986) 2356-2359.
[13] K. Hirose, W. Keim, Olefin oligomerization with nickel PO chelate complexes, J. Mol. Catal., 73 (1992) 271-276.
[14] L.K. Johnson, C.M. Killian, M. Brookhart, New Pd(II)- and Ni(II)-Based Catalysts for Polymerization of Ethylene and .alpha.-Olefins, J. Am. Chem. Soc., 117 (1995) 6414-6415.
[15] C. Wang, S. Friedrich, T.R. Younkin, R.T. Li, R.H. Grubbs, D.A. Bansleben, M.W. Day, Neutral Nickel(II)-Based Catalysts for Ethylene Polymerization, Organometallics, 17 (1998) 3149-3151.
[16] T.R. Younkin, E.F. Connor, J.I. Henderson, S.K. Friedrich, R.H. Grubbs, D.A. Bansleben, Neutral, Single-Component Nickel (II) Polyolefin Catalysts That Tolerate Heteroatoms, Science, 287 (2000) 460.
[17] E.F. Connor, T.R. Younkin, J.I. Henderson, S. Hwang, R.H. Grubbs, W.P. Roberts, J.J. Litzau, Linear functionalized polyethylene prepared with highly active neutral Ni(II) complexes, J. Polym. Sci. A Polym. Chem., 40 (2002) 2842-2854.
[18] Z. Guan, P.M. Cotts, E.F. McCord, S.J. McLain, Chain Walking: A New Strategy to Control Polymer Topology, Science, 283 (1999) 2059.
[19] I. Pierro, G. Zanchin, E. Parisini, J. Martí-Rujas, M. Canetti, G. Ricci, F. Bertini, G. Leone, Chain-Walking Polymerization of α-Olefins by α-Diimine Ni(II) Complexes: Effect of Reducing the Steric Hindrance of Ortho- and Para-Aryl Substituents on the Catalytic Behavior, Monomer Enchainment, and Polymer Properties, Macromolecules, 51 (2018) 801-814.
[20] F. Wang, C. Chen, A continuing legend: the Brookhart-type α-diimine nickel and palladium catalysts, Polym. Chem., 10 (2019) 2354-2369.
[21] J.A. Ewen, Mechanisms of stereochemical control in propylene polymerizations with soluble Group 4B metallocene/methylalumoxane catalysts, J. Am. Chem. Soc., 106 (1984) 6355-6364.
[22] W. Kaminsky, K. Külper, H.H. Brintzinger, F.R.W.P. Wild, Polymerization of Propene and Butene with a Chiral Zirconocene and Methylalumoxane as Cocatalyst, Angew. Chem. Int. Ed. Engl., 24 (1985) 507-508.
[23] J.A. Ewen, Symmetry rules and reaction mechanisms of Ziegler-Natta catalysts, J. Mol. Catal. A Chem., 128 (1998) 103-109.
[24] J.A. Ewen, R.L. Jones, A. Razavi, J.D. Ferrara, Syndiospecific propylene polymerizations with Group IVB metallocenes, J. Am. Chem. Soc., 110 (1988) 6255-6256.
[25] S. Miyake, Y. Okumura, S. Inazawa, Highly Isospecific Polymerization of Propylene with Unsymmetrical Metallocene Catalysts, Macromolecules, 28 (1995) 3074-3079.
[26] A. Razavi, D. Vereecke, L. Peters, K. Den Dauw, L. Nafpliotis, J.L. Atwood, in: G. Fink, R. Mülhaupt, H.H. Brintzinger (Eds.) Ziegler Catalysts, Springer - Verlag, Berlin, 1995, pp. 111.
[27] A. Razavi, U. Thewalt, Site selective ligand modification and tactic variation in polypropylene chains produced with metallocene catalysts, Coord. Chem. Rev., 250 (2006) 155-169.
[28] S.A. Miller, J.E. Bercaw, Isotactic−Hemiisotactic Polypropylene from C1-Symmetric ansa-Metallocene Catalysts: A New Strategy for the Synthesis of Elastomeric Polypropylene, Organometallics, 21 (2002) 934-945.
[29] G. Lanza, I.L. Fragalà, T.J. Marks, Ligand Substituent, Anion, and Solvation Effects on Ion Pair Structure, Thermodynamic Stability, and Structural Mobility in "Constrained Geometry" Olefin Polymerization Catalysts: an Ab Initio Quantum Chemical Investigation, J. Am. Chem. Soc., 122 (2000) 12764-12777.

[30] J. Zhou, S.J. Lancaster, D.A. Walker, S. Beck, M. Thornton-Pett, M. Bochmann, Synthesis, Structures, and Reactivity of Weakly Coordinating Anions with Delocalized Borate Structure: The Assessment of Anion Effects in Metallocene Polymerization Catalysts, J. Am. Chem. Soc., 123 (2001) 223-237.
[31] M.-C. Chen, J.A.S. Roberts, T.J. Marks, Marked Counteranion Effects on Single-Site Olefin Polymerization Processes. Correlations of Ion Pair Structure and Dynamics with Polymerization Activity, Chain Transfer, and Syndioselectivity, J. Am. Chem. Soc., 126 (2004) 4605-4625.
[32] A. Macchioni, Ion pairing in transition-metal organometallic chemistry, Chem. Rev., 105 (2005) 2039-2074.
[33] J.L. Eilertsen, J.A. Støvneng, M. Ystenes, E. Rytter, Activation of Metallocenes for Olefin Polymerization As Monitored by IR Spectroscopy, Inorg. Chem., 44 (2005) 4843-4851.
[34] Y. Gao, J. Chen, Y. Wang, D.B. Pickens, A. Motta, Q.J. Wang, Y.-W. Chung, T.L. Lohr, T.J. Marks, Highly branched polyethylene oligomers via group IV-catalysed polymerization in very nonpolar media, Nat. Catal., 2 (2019) 236-242.
[35] F. Zaccaria, P.H.M. Budzelaar, R. Cipullo, C. Zuccaccia, A. Macchioni, V. Busico, C. Ehm, Reactivity Trends of Lewis Acidic Sites in Methylaluminoxane and Some of Its Modifications, Inorg. Chem., 59 (2020) 5751-5759.
[36] F. Zaccaria, L. Sian, C. Zuccaccia, A. Macchioni, Chapter One - Ion pairing in transition metal catalyzed olefin polymerization, 73 (2020) 1-78.
[37] R. Parveen, T.R. Cundari, J.M. Younker, G. Rodriguez, Computational Assessment of Counterion Effect of Borate Anions on Ethylene Polymerization by Zirconocene and Hafnocene Catalysts, Organometallics, 39 (2020) 2068-2079.
[38] E. Groppo, K. Seenivasan, C. Barzan, The potential of spectroscopic methods applied to heterogeneous catalysts for olefin polymerization, Catal. Sci. Technol., 3 (2013) 858-878.
[39] H. Topsøe, Developments in operando studies and in situ characterization of heterogeneous catalysts, J. Catal., 216 (2003) 155-164.
[40] B.M. Weckhuysen, Determining the active site in a catalytic process: Operando spectroscopy is more than a buzzword, Phys. Chem. Chem. Phys., 5 (2003) 4351-4360.
[41] M.A. Bañares, Operando methodology: combination of in situ spectroscopy and simultaneous activity measurements under catalytic reaction conditions, Catal. Today, 100 (2005) 71-77.
[42] M.A. Bañares, Operando Spectroscopy: the Knowledge Bridge to Assessing Structure–Performance Relationships in Catalyst Nanoparticles, Adv. Mater., 23 (2011) 5293-5301.
[43] A. Chakrabarti, M.E. Ford, D. Gregory, R. Hu, C.J. Keturakis, S. Lwin, Y. Tang, Z. Yang, M. Zhu, M.A. Bañares, I.E. Wachs, A decade+ of operando spectroscopy studies, Catal. Today, 283 (2017) 27-53.
[44] K. Soga, T. Shiono, Y. Doi, Influence of internal and external donors on activity and stereospecificity of Ziegler-Natta catalysts, Makromol. Chem., 189 (1988) 1531-1541.
[45] M.C. Sacchi, I. Tritto, C. Shan, R. Mendichi, L. Noristi, Role of the Pair of Internal and External Donors in MgCl2-Supported Ziegler-Natta Catalysts, Macromolecules, 24 (1991) 6823-6826.
[46] E. Albizzati, U. Giannini, G. Collina, L. Noristi, L. Resconi, Catalysts and polymerizations, in: E.P.J. Moore (Ed.) Polypropylene Handbook, Hanser-Gardner Publications, Cincinnati (Ohio, USA), 1996.
[47] J. Kumawat, V.K. Gupta, Fundamental aspects of heterogeneous Ziegler–Natta olefin polymerization catalysis: an experimental and computational overview, Polym. Chem., 11 (2020) 6107-6128.
[48] M. Ratanasak, T. Rungrotmongkol, O. Saengsawang, S. Hannongbua, V. Parasuk, Towards the design of new electron donors for Ziegler-Natta catalyzed propylene polymerization using QSPR modeling, Polymer, 56 (2015) 340-345.
[49] A. Andoni, J.C. Chadwick, S. Milani, H. Niemantsverdriet, P.C. Thune, Introducing a new surface science model for Ziegler-Natta catalysts: Preparation, basic characterization and testing, J. Catal., 247 (2007) 129-136.
[50] A. Andoni, J.C. Chadwick, H.J.W. Niemantsverdriet, P.C. Thune, The Role of Electron Donors on Lateral Surfaces of MgCl2-Supported Ziegler-Natta Catalysts: Observation by AFM and SEM, J. Catal., 257 (2008) 81-86.
[51] G. Morini, E. Albizzati, G. Balbontin, I. Mingozzi, M.C. Sacchi, F. Forlini, I. Tritto, Microstructure Distribution of Polypropylenes Obtained in the Presence of Traditional Phthalate/Silane and Novel Diether

Donors: A Tool for Understanding the Role of Electron Dnors in MgCl2-Supported Ziegler-Natta Catalysts. , Macromolecules, 29 (1996) 5770−5776.
[52] M.C. Sacchi, F. Forlini, I. Tritto, R. Mendichi, G. Zannoni, L. Noristi, Activation Effect of Alkoxysilanes as External Donors in MgCl2-Supported Ziegler-Natta Catalysts, Macromolecules, 25 (1992) 5914-5918.
[53] T. Taniike, M. Terano, Coadsorption and support-mediated interaction of ti species with ethyl benzoate in MgCl2-Supported heterogeneous ziegler-natta catalysts studied by density functional calculations, Macromol. Rapid Commun., 28 (2007) 1918-1922.
[54] J.C. Chadwick, G.M.M. Vankessel, O. Sudmeijer, Regiospecificity and Stereospecificity in Propene Polymerization with Mgcl2-Supported Ziegler-Natta Catalysts - Effects of Hydrogen and the External Donor, Macromol. Chem. Phys., 196 (1995) 1431-1437.
[55] V. Busico, J.C. Chadwick, R. Cipullo, S. Ronca, G. Talarico, Propene/ethene-[1-C-13] copolymerization as a tool for investigating catalyst regioselectivity. MgCl2/internal donor/TiCl4-external donor/AlR3 systems, Macromolecules, 37 (2004) 7437-7443.
[56] A. Vittoria, A. Meppelder, N. Friederichs, V. Busico, R. Cipullo, Ziegler–Natta Catalysts: Regioselectivity and “Hydrogen Response”, ACS Catal., 10 (2020) 644-651.
[57] K. Soga, T. Shiono, Y. Doi, Effect of ethyl benzoate on the copolymerization of ethylene with higher α-olefins over TiCl4/MgCl2 catalytic systems, Polym. Bull., 10 (1983) 168-174.
[58] J.C. Chadwick, A. Miedema, O. Sudmeijer, Hydrogen Activation in Propene Polymerization with Mgcl2-Supported Ziegler-Natta Catalysts - the Effect of the External Donor, Macromol. Chem. Phys., 195 (1994) 167-172.
[59] J.C. Chadwick, G. Morini, G. Balbontin, I. Mingozzi, E. Albizzati, O. Sudmeijer, Propene polymerization with MgCl2-supported catalysts: Effects of using a diether as external donor, Macromol. Chem. Phys., 198 (1997) 1181-1188.
[60] P. Corradini, V. Barone, R. Fusco, G. Guerra, Analysis of models for the Ziegler-Natta stereospecific polymerization on the basis of non-bonded interactions at the catalytic site - I. The Cossee model, Eur. Polym. J., 15 (1979) 1133-1141.
[61] P. Corradini, V. Barone, R. Fusco, G. Guerra, A possible model of catalytic sites for the stereospecific polymerization of alpha-olefins on 1st-generation and supported Ziegler-Natta catalysts, Gazz. Chim. Ital., 113 (1983) 601-607.
[62] A. Vittoria, A. Meppelder, N. Friederichs, V. Busico, R. Cipullo, Demystifying Ziegler-Natta Catalysts: The Origin of Stereoselectivity, ACS Catal., 7 (2017) 4509-4518.
[63] P. Corradini, G. Guerra, L. Cavallo, Do New Century Catalysts Unravel the Mechanism of Stereocontrol of Old Ziegler-Natta catalysts?, Acc. Chem. Res., 37 (2004) 231-241.
[64] M. Terano, T. Kataoka, A study on the states of ethyl benzoate and TiCl4 in MgCl2-supported high-yield catalysts, Makromol. Chem. , 188 (1987) 1477- 1487.
[65] G. Monaco, M. Toto, G. Guerra, P. Corradini, L. Cavallo, Geometry and stability of titanium chloride species adsorbed on the (100) and (110) cuts of the MgCl2 support of the heterogeneous Ziegler-Natta catalysts, Macromolecules, 33 (2000) 8953-8962.
[66] M. D'Amore, R. Credendino, P.H.M. Budzelaar, M. Causá, V. Busico, A periodic hybrid DFT approach (including dispersion) to MgCl2-supported Ziegler–Natta catalysts – 1: TiCl4 adsorption on MgCl2 crystal surfaces, J. Catal., 286 (2012) 103−110.
[67] M. D'Amore, K.S. Thushara, A. Piovano, M. Causà, S. Bordiga, E. Groppo, Surface Investigation and Morphological Analysis of Structurally Disordered MgCl2 and MgCl2/TiCl4 Ziegler–Natta Catalysts, ACS Catal., 6 (2016) 5786–5796.
[68] T. Taniike, M. Terano, Coadsorption model for first-principle description of roles of donors in heterogeneous Ziegler-Natta propylene polymerization, J. Catal., 293 (2012) 39-50.
[69] S. Shetty, Synergistic, reconstruction and bonding effects during the adsorption of internal electron donors and TiCl4 on MgCl2 surface: A periodic-DFT investigation, Surf. Sci., 653 (2016) 55-65.
[70] T. Iijima, T. Shimizu, A. Goto, K. Deguchi, T. Nakai, R. Ohashi, M. Saito, 47,49Ti solid-state NMR and DFT study of Ziegler-Natta catalyst: Adsorption of TiCl4 molecule onto the surface of MgCl2, J. Phys. Chem. Solids, 135 (2019) 109088.

[71] M.C. Sacchi, F. Forlini, I. Tritto, P. Locatelli, Stereochemistry of the initiation step in Ziegler-Natta catalysts containing dialkyl propane diethers: a tool for distinguishing the role of internal and external donors, Macromol. Symp., 89 (1995) 91-100.
[72] M.C. Sacchi, I. Tritto, P. Locatelli, Stereochemical investigation of the effect of lewis bases in heterogeneous ziegler-natta initiator systems, Prog. Polym. Sci., 16 (1991) 331-360.
[73] M. Seth, T. Ziegler, Polymerization Properties of a Heterogeneous Ziegler-Natta Catalyst Modified by a Base: A Theoretical Study, Macromolecules, 36 (2003) 6613-6623.
[74] Z. Flisak, Multidentate Tetrahydrofurfuryloxide Ligand in a Ziegler−Natta Catalyst Studied by Molecular Modeling, Macromolecules, 41 (2008) 6920-6924.
[75] M.L. Ferreira, N.J. Castellani, D.E. Damiani, A. Juan, The Co-adsorption of tetramethylpiperidine and TiCl4 on β-MgCl2. A theoretical study of a Ziegler-Natta pre-catalyst, J. Mol. Catal. A Chem., 122 (1997) 25-37.
[76] Ø. Bache, M. Ystenes, Double-Chamber Flow Cell for in Situ Infrared Spectroscopy Studies of Chemical Reactions in Ziegler-Natta Catalyst Systems, Applied Spectroscopy, 48 (1994) 985-993.
[77] E. Rytter, O. Nirisen, M. Ystenes, H.A. Oye, FTIR Spectroscopy of Ethyl Benzoate-Titanium Tetrachloride Complexes with Application to Supported Ziegler-Natta Catalysts, Mikrochim. Acta, (1988) 85-87.
[78] L. Cavallo, S. Del Piero, J.-M. Ducéré, R. Fedele, A. Melchior, G. Morini, F. Piemontesi, M. Tolazzi, Key Interactions in Heterogeneous Ziegler-Natta Catalytic Systems: Structure and Energetics of TiCl4-Lewis Base Complexes, J. Phys. Chem. C, 111 (2007) 4412-4419.
[79] D.V. Stukalov, V.A. Zakharov, I.L. Zilberberg, Adsorption species of ethyl benzoate in MgCl2-supported ziegler-natta catalysts. A density functional theory study, J. Phys. Chem. C, 114 (2010) 429-435.
[80] A. Correa, F. Piemontesi, G. Morini, L. Cavallo, Key Elements in the Structure and Function Relationship of the MgCl2/TiCl4/Lewis base Ziegler-Natta Catalytic System, Macromolecules, 40 (2007) 9181-9189.
[81] V. Busico, R. Cipullo, G. Monaco, G. Talarico, M. Vacatello, J.C. Chadwick, A.L. Segre, O. Sudmeijer, High-resolution C-13 NMR configurational analysis of polypropylene made with MgCl2-supported Ziegler-Natta catalysts. 1. The "model" system MgCl2/TiCl4-2,6-dimethylpyridine/Al(C2H5)(3), Macromolecules, 32 (1999) 4173-4182.
[82] A.S. Bazhenov, P. Denifl, T. Leinonen, A. Pakkanen, M. Linnolahti, T.A. Pakkanen, Modeling Coadsorption of Titanium Tetrachloride and Bidentate Electron Donors on Magnesium Dichloride Support Surfaces, J. Phys. Chem. C, 118 (2014) 27878-27883.
[83] X. Guo, L. Cui, Y. Wang, J. Yi, J. Sun, Z. Liu, B. Liu, Mechanistic Study on Effect of Electron Donors in Propylene Polymerization Using the Ziegler–Natta Catalyst, J. Phys. Chem. C, 125 (2021) 8533-8542.
[84] C.B. Yang, C.C. Hsu, Y.S. Park, H.F. Shurvell, Infrared characterization of MgCl2 supported Ziegler-Natta catalysts with monoester and diester as a modifier, Eur. Polym. J., 30 (1994) 205-214.
[85] A.G. Potapov, G.D. Bukatov, V.A. Zakharov, DRIFT Study of Internal Donors in Supported Ziegler-Natta Catalysts, J. Mol. Catal. A: Chem., 246 (2006) 248-254.
[86] A.G. Potapov, G.D. Bukatov, V.A. Zakharov, DRIFTS study of the interaction of the AlEt3 cocatalyst with the internal donor ethyl benzoate in supported Ziegler-Natta catalysts, J. Mol. Catal. A: Chem., 301 (2009) 18-23.
[87] A.G. Potapov, G.D. Bukatov, V.A. Zakharov, DRIFTS Study of the Interaction of the Internal Donor in TiCl4/di-n-Butyl Phthalate/MgCl2 Catalysts with AlEt3 Cocatalyst, J. Mol. Catal. A: Chem., 316 (2010) 95-99.
[88] D.V. Stukalov, V.A. Zakharov, A.G. Potapov, G.D. Bukatov, Supported Ziegler-Natta catalysts for Propylene Polymerization. Study of Surface Species Formed at Interaction of Electron Donors and TiCl4 with Activated MgCl2, J. Catal., 266 (2009) 39-49.
[89] A.V. Cheruvathur, E.H.G. Langner, J.W. Niemantsverdriet, P.C. Thüne, In Situ ATR-FTIR Studies on MgCl2-Diisobutyl Phthalate Interactions in Thin Film Ziegler-Natta Catalysts, Langmuir, 28 (2012) 2643-2651.
[90] A. Piovano, M. D'Amore, K.S. Thushara, E. Groppo, Spectroscopic Evidences for TiCl4/Donor Complexes on the Surface of MgCl2-Supported Ziegler-Natta Catalysts, J. Phys. Chem. C, 122 (2018) 5615-5626.
[91] M. Kioka, H. Kitani, N. Kashiwa, Process for producing olefin polymers or copolymers, US 4330649 (1982).
[92] M. Terano, H. Soga, K. Kimura, Catalyst for Polymerization of Olefins, US 4,829,037 (1989).

[93] M. Ystenes, E. Rytter, FT-IR and Raman spectra of ethyl benzoate. Assignment based on differences between phases, complexation to titanium tetrachloride, isotopic shifts and normal coordinate analysis, Spectrochim. Acta, Part A, 45 (1989) 1127-1135.
[94] M. Ystenes, E. Rytter, Fourier transform infrared spectra of three titanium tetrachloride-ethyl benzoate complexes. Assignment based on five isotopic homologues and extension of the ethyl benzoate force field, Spectrochim. Acta, Part A, 48 (1992) 543-555.
[95] C.N.R. Rao, R. Venkataraghavan, Infrared spectra of substituted benzoyl chlorides and benzoyl bromides. Explanation of the anomalous carbonyl band-splittings, Spectrochim. Acta, 18 (1962) 273-278.
[96] E. Ortiz, J.F. Bertran, L. Ballester, Substituent effect on Fermi resonance in p-substituted benzoyl chlorides, Spectrochim. Acta, Part A, 27 (1971) 1713-1720.
[97] R. Credendino, D. Liguori, G. Morini, L. Cavallo, Investigating phthalate and 1,3-diether coverage and dynamics on the (104) and (110) surfaces of MgCl2-supported Ziegler-Natta catalysts, J. Phys. Chem. C, 118 (2014) 8050-8058.
[98] R. Credendino, J.T.M. Pater, D. Liguori, G. Morini, L. Cavallo, Investigating Alkoxysilane Coverage and Dynamics on the (104) and (110) Surfaces of MgCl2-Supported Ziegler−Natta Catalysts, J. Phys. Chem. C, 116 (2012) 22980−22986.
[99] Y. Chen, P. Liang, Z. Yue, W. Li, C. Dong, B. Jiang, J. Wang, Y. Yang, Entanglement Formation Mechanism in the POSS Modified Heterogeneous Ziegler–Natta Catalysts, Macromolecules, 52 (2019) 7593-7602.
[100] P. Liang, W. Li, Y. Chen, C. Dong, Q. Zhou, Y. Feng, M. Chen, J. Dai, C. Ren, B. Jiang, J. Wang, Y. Yang, Revealing the Dynamic Behaviors of Tetrahydrofuran for Tailoring the Active Species of Ziegler–Natta Catalysts, ACS Catal., (2021) 4411-4421.
[101] W. Kaminsky, Polyolefins: 50 years after Ziegler and Natta I, Springer, Berlin, 2013.
[102] S. Parodi, R. Nocci, U. Giannini, P.C. Barbe, U. Scata, Components and catalysts for the polymerization of olefins, EP0045977B2 (1982).
[103] G. Singh, S. Kaur, U. Makwana, R.B. Patankar, V.K. Gupta, Influence of Internal Donors on the Performance and Structure of MgCl2 Supported Titanium Catalysts for Propylene Polymerization, Macromol. Chem. Phys., 210 (2009) 69-76.
[104] N.N. Chumachenko, V.A. Zakharov, G.D. Bukatov, S.A. Sergeev, A study of the formation process of titanium–magnesium catalyst for propylene polymerization, Appl. Catal. A: Gen., 469 (2014) 512-516.
[105] U. Makwana, D.G. Naik, G. Singh, V. Patel, H.R. Patil, V.K. Gupta, Nature of Phthalates as Internal Donors in High Performance MgCl2 Supported Titanium Catalysts, Catal. Lett., 131 (2009) 624-631.
[106] G.G. Arzoumanidis, N.M. Karayannis, Infrared spectral characterization of supported propene polymerization catalysts: A link to catalyst performance, Appl. Catal., 76 (1991) 221-231.
[107] A. Dashti, A. Ramazani Sa, Y. Hiraoka, S.Y. Kim, T. Taniike, M. Terano, Kinetic and morphological study of a magnesium ethoxide-based Ziegler-Natta catalyst for propylene polymerization, Polym. Int., 58 (2009) 40-45.
[108] Y. Hiraoka, S.Y. Kim, A. Dashti, T. Taniike, M. Terano, Similarities and Differences of the Active Sites in Basic and Advanced MgCl2-Supported Ziegler-Natta Propylene Polymerization Catalysts, Macromol. React. Eng., 4 (2010) 510-515.
[109] A. Piovano, T. Wada, A. Amodio, G. Takasao, M. Terano, P. Chammingkwan, E. Groppo, T. Taniike, On the formation of highly active Ziegler-Natta catalysts clarified by a multifaceted characterization approach, ACS Catal., (2021) submitted.
[110] T. Taniike, M. Terano, The use of donors to increase the isotacticity of polypropylene., in: W. Kaminsky (Ed.) Polyolefins: 50 Years after Ziegler and Natta I, Springer, Berlin, 2013, pp. 81-97.
[111] T. Wada, A. Thakur, P. Chammingkwan, M. Terano, T. Taniike, A. Piovano, E. Groppo, Structural Disorder of Mechanically Activated δ-MgCl2 Studied by Synchrotron X-ray Total Scattering and Vibrational Spectroscopy, Catalysts, 10 (2020) 1089.
[112] M.S. Kuklin, A.S. Bazhenov, P. Denifl, T. Leinonen, M. Linnolahti, T.A. Pakkanena, Stabilization of magnesium dichloride surface defects by mono- and bidentate donors, Surf. Sci., 635 (2015) 5–10.
[113] K. Vanka, G. Singh, D. Iyer, V.K. Gupta, DFT Study of Lewis Base Interactions with the MgCl2 Surface in the Ziegler−Natta Catalytic System: Expanding the Role of the Donors, J. Phys. Chem. C, 114 (2010) 15771-15781.

[114] J.C.W. Chien, J.-C. Wu, Magnesium-chloride-supported high-mileage catalysts for olefin polymerization. II. Reactions between aluminum alkyl and promoters, J. Polym. Sci. Polym. Chem. Ed., 20 (1982) 2445-2460.
[115] A. Vittoria, G. Antinucci, F. Zaccaria, R. Cipullo, V. Busico, Monitoring the Kinetics of Internal Donor Clean-up from Ziegler–Natta Catalytic Surfaces: An Integrated Experimental and Computational Study, J. Phys. Chem. C, 124 (2020) 14245-14252.
[116] F. Zaccaria, A. Vittoria, A. Correa, C. Ehm, P.H.M. Budzelaar, V. Busico, R. Cipullo, Internal Donors in Ziegler–Natta Systems: is Reduction by AlR3 a Requirement for Donor Clean-Up?, ChemCatChem, 10 (2018) 984-988.
[117] Y. Fang, B. Liu, M. Terano, Various activation procedures of Phillips catalyst for ethylene polymerization, Kinet. Catal., 47 (2006) 295-302.
[118] B. Liu, H. Nakatani, M. Terano, New aspects of the induction period of ethene polymerization using Phillips CrOx/SiO2 catalyst probed by XPS, TPD and EPMA, J. Mol. Catal. A: Chem., 184 (2002) 387-398.
[119] B.P. Liu, H. Nakatani, M. Terano, Mechanistic implications of the unprecedented transformations of ethene into propene and butene over Phillips CrO_x/SiO_2 catalyst during induction period, J. Mol. Catal. A, 201 (2003) 189-197.
[120] M. Gierada, J. Handzlik, Computational insights into reduction of the Phillips CrOx/SiO2 catalyst by ethylene and CO, J. Catal., 359 (2018) 261-271.
[121] A. Chakrabarti, M. Gierada, J. Handzlik, I.E. Wachs, Operando Molecular Spectroscopy During Ethylene Polymerization by Supported CrOx/SiO2 Catalysts: Active Sites, Reaction Intermediates, and Structure-Activity Relationship, Top. Catal., 59 (2016) 725-739.
[122] K.C. Potter, C.W. Beckerle, F.C. Jentoft, E. Schwerdtfeger, M.P. McDaniel, Reduction of the Phillips catalyst by various olefins: Stoichiometry, thermochemistry, reaction products and polymerization activity, J. Catal., 344 (2016) 657-668.
[123] S. Krimm, C.Y. Liang, G.B.B.M. Sutherland, Infrared Spectra of High Polymers. II. Polyethylene, J. Chem. Phys., 25 (1956) 549-562.
[124] J.R. Nielsen, A.H. Woollett, Vibrational Spectra of Polyethylenes and Related Substances, J. Chem. Phys., 26 (1957) 1391-1401.
[125] C. Barzan, A. Piovano, L. Braglia, G.A. Martino, C. Lamberti, S. Bordiga, E. Groppo, Ligands Make the Difference! Molecular Insights into CrVI/SiO2 Phillips Catalyst during Ethylene Polymerization, J. Am. Chem. Soc., 139 (2017) 17064–17073.
[126] J. Joseph, K.C. Potter, M.J. Wulfers, E. Schwerdtfeger, M.P. McDaniel, F.C. Jentoft, Products of the initial reduction of the Phillips catalyst by olefins, J. Catal., 377 (2019) 550-564.
[127] H.L. Krauss, H. Stach, Chrom(II) als wirksamer bestandteil des Phillips Katalysators zur Äthylenpolymerisation, Inorg. Nucl. Chem. Lett., 4 (1968) 393-397.
[128] A. Zecchina, E. Garrone, G. Ghiotti, C. Morterra, E. Borello, On the chemistry of Silica supported chromium ions. I. Characterization of the samples, J. Phys. Chem., 79 (1975) 966-972.
[129] B. Rebenstorf, On the Catalytic Activity of Mononuclear and Dinuclear Chromium(II)-A Surface Species on Silica Gel, Acta Chem. Scand. A, 43 (1989) 413.
[130] B. Rebenstorf, R. Larsson, Why do homogeneous analogs of Phillips (CrO_3/SiO_2) and Union Carbide (chromocene/SiO_2) polyethylene catalysts fail? Some answers from IR investigations., J. Mol. Catal., 11 (1981) 247-256.
[131] G. Ghiotti, E. Garrone, A. Zecchina, IR investigation of polymerization centres of the Phillips catalyst, J. Mol. Catal., 46 (1988) 61-77.
[132] W. Tischtschenko, Chem. Zentralbl., 77 (1906) 1309.
[133] T. Ooi, T. Miura, Y. Itagaki, H. Ichikawa, K. Maruoka, Catalytic Meerwein-Ponndorf-Verley (MPV) and Oppenauer (OPP) reactions: Remarkable acceleration of the hydride transfer by powerful bidentate aluminum alkoxides, Synthesis, 2 (2002) 279-291.
[134] V. Crocellà, G. Cerrato, G. Magnacca, C. Morterra, F. Cavani, L. Maselli, S. Passeri, Gas-phase phenol methylation over Mg/Me/O (Me = Al, Cr, Fe) catalysts: Mechanistic implications due to different acid-base and dehydrogenating properties, Dalton Trans., 39 (2010) 8527-8537.

[135] Y. Hoshimoto, M. Ohashi, S. Ogoshi, Nickel-Catalyzed Selective Conversion of Two Different Aldehydes to Cross-Coupled Esters, J. Am. Chem. Soc., 133 (2011) 4668-4671.
[136] L. Mino, C. Barzan, G.A. Martino, A. Piovano, G. Spoto, A. Zecchina, E. Groppo, Photoinduced Ethylene Polymerization on the CrVI/SiO2 Phillips Catalyst, J. Phys. Chem. C, 123 (2019) 8145–8152.
[137] M. Anpo, I. Tanahashi, Y. Kubokawa, Photoreducibility of supported metal oxides and lifetimes of their excited triplet states, J. Phys. Chem., 86 (1982) 1-3.
[138] M. Anpo, T.-H. Kim, M. Matsuoka, The design of Ti-, V-, Cr-oxide single-site catalysts within zeolite frameworks and their photocatalytic reactivity for the decomposition of undesirable molecules—The role of their excited states and reaction mechanisms, Catal. Today, 142 (2009) 114–124.
[139] M. Anpo, J.M. Thomas, Single-site photocatalytic solids for the decomposition of undesirable molecules, Chem. Commun., (2006) 3273-3278.
[140] O. Berg, M.S. Hamdy, T. Maschmeyer, J.A. Moulijn, M. Bonn, G. Mul, On the Wavelength-Dependent Performance of Cr-Doped Silica in Selective Photo-Oxidation, J. Phys. Chem. C, 112 (2008) 5471-5475.
[141] D.S. McGuinness, N.W. Davies, J. Horne, I. Ivanov, Unraveling the Mechanism of Polymerization with the Phillips Catalyst, Organometallics, 29 (2010) 6111-6116.
[142] M.F. Delley, M.P. Conley, C. Copéret, Polymerization on CO-Reduced Phillips Catalyst initiates through the C–H bond Activation of Ethylene on Cr–O Sites, Catal. Lett., 144 (2014) 805-808.
[143] C. Brown, J. Krzystek, R. Achey, A. Lita, R. Fu, R.W. Meulenberg, M. Polinski, N. Peek, Y. Wang, L.J. Van De Burgt, S. Profeta, A.E. Stiegman, S.L. Scott, Mechanism of Initiation in the Phillips Ethylene Polymerization Catalyst: Redox Processes Leading to the Active Site, ACS Catal., 5 (2015) 5574-5583.
[144] C. Brown, A. Lita, Y. Tao, N. Peek, M. Crosswhite, M. Mileham, J. Krzystek, R. Achey, R. Fu, J.K. Bindra, M. Polinski, Y. Wang, L.J. Van De Burgt, D. Jeffcoat, S. Profeta, A.E. Stiegman, S.L. Scott, Mechanism of Initiation in the Phillips Ethylene Polymerization Catalyst: Ethylene Activation by Cr(II) and the Structure of the Resulting Active Site, ACS Catal., 7 (2017) 7442-7455.
[145] B.M. Weckhuysen, L.M. Deridder, R.A. Schoonheydt, A quantitative diffuse reflectance spectroscopy study of supported chromium catalysts, J. Phys. Chem., 97 (1993) 4756-4763.
[146] A. Budnyk, A. Damin, C. Barzan, E. Groppo, C. Lamberti, S. Bordiga, A. Zecchina, Cr-doped porous silica glass as a model material to describe Phillips catalyst properties, J. Catal., 308 (2013) 319-327.
[147] B.N. Figgis, Introduction to ligand fields, John Wiley & Sons, New York, 1966.
[148] E.A. Benham, P.D. Smith, E.T. Hsieh, M.P. McDaniel, Mixed Organo/Oxide Chromium Polymerization Catalysts, J. Macromol. Sci. Chem., 25 (1988) 259-283.
[149] T. Wada, T. Funako, P. Chammingkwan, A. Thakur, A. Matta, M. Terano, T. Taniike, Structure-performance relationship of Mg(OEt)2-based Ziegler-Natta catalysts, J. Catal., 389 (2020) 525-532.
[150] A. Piovano, P. Pletcher, M.E.Z. Velthoen, S. Zanoni, S.-H. Chung, K. Bossers, M.K. Jongkind, G. Fiore, E. Groppo, B.M. Weckhuysen, Genesis of MgCl2-based Ziegler-Natta Catalysts as Probed with Operando Spectroscopy, ChemPhysChem, 19 (2018) 2662-2671.
[151] A. Piovano, M. Signorile, L. Braglia, P. Torelli, A. Martini, T. Wada, G. Takasao, T. Taniike, E. Groppo, Electronic Properties of Ti Sites in Ziegler−Natta Catalysts, ACS Catal., 11 (2021) 9949–9961.
[152] N. Bahri-Laleh, A. Hanifpour, S.A. Mirmohammadi, A. Poater, M. Nekoomanesh-Haghighi, G. Talarico, L. Cavallo, Computational modeling of heterogeneous Ziegler-Natta catalysts for olefins polymerization, Prog. Polym. Sci., 84 (2018) 89-114.
[153] G. Takasao, T. Wada, A. Thakur, P. Chammingkwan, M. Terano, T. Taniike, Insight into structural distribution of heterogeneous Ziegler–Natta catalyst from non-empirical structure determination, J. Catal., 394 (2021) 299-306.
[154] G. Ghiotti, E. Garrone, A. Zecchina, An infrared study of CO/C_2H_4 coadsorption and reaction on silica-supported Cr(II) ions, J. Mol. Catal., 65 (1991) 73-83.
[155] A. Zecchina, G. Spoto, G. Ghiotti, E. Garrone, Cr^{2+} ions grafted to silica and silicalite surfaces - FTIR characterization and ethylene polymerization activity, J. Mol. Catal., 86 (1994) 423-446.
[156] A.B. Gaspar, R.L. Martins, M. Schmal, L.C. Dieguez, Characterization of Cr^{2+} and ethylene polymerization on Cr/SiO_2 catalysts, J. Mol. Catal. A, 169 (2001) 105-112.
[157] A.B. Gaspar, J.L.F. Brito, L.C. Dieguez, Characterization of chromium species in catalysts for dehydrogenation and polymerization, J. Mol. Catal. A, 203 (2003) 251-266.

[158] E. Groppo, C. Lamberti, S. Bordiga, G. Spoto, A. Zecchina, The structure of active centers and the ethylene polymerization mechanism on the Cr/SiO_2 catalyst: a frontier for the characterization methods, Chem. Rev., 105 (2005) 115-184.
[159] E. Groppo, G.A. Martino, A. Piovano, C. Barzan, The active sites in the Phillips catalysts: origins of a lively debate and a vision for the future, ACS Catal., 8 (2018) 10846-10863.
[160] G. Spoto, S. Bordiga, A. Zecchina, D. Cocina, E.N. Gribov, L. Regli, E. Groppo, C. Lamberti, New frontier in transmission IR spectroscopy of molecules adsorbed on high surface area solids: Experiments below liquid nitrogen temperature, Catal. Today, 113 (2006) 65-80.
[161] D. Gianolio, E. Groppo, J.G. Vitillo, A. Damin, S. Bordiga, A. Zecchina, C. Lamberti, Direct evidence of adsorption induced CrII mobility on the SiO2 surface upon complexation by CO, Chem. Commun., 46 (2010) 976–978.
[162] A. Damin, F. Bonino, S. Bordiga, E. Groppo, C. Lamberti, A. Zecchina, Vibrational Properties of CrII Centers on Reduced Phillips Catalysts Highlighted by Resonant Raman Spectroscopy, ChemPhysChem, 7 (2006) 342-344.
[163] S. Veliah, K.-H. Xiang, R. Pandey, J.M. Recio, J.M. Newsam, Density Functional Study of Chromium Oxide Clusters: Structures, Bonding, Vibrations, and Stability, J. Phys. Chem. B, 102 (1998) 1126-1135.
[164] A. Bensalem, B.M. Weckhuysen, R.A. Schoonheydt, In situ diffuse reflectance spectroscopy of supported chromium oxide catalysts: Kinetics of the reduction process with carbon monoxide, J. Phys. Chem. B, 101 (1997) 2824-2829.
[165] K.C.H. Tijssen, E.S. Blaakmeer, A.P.M. Kentgens, Solid-state NMR studies of Ziegler–Natta and metallocene catalysts, Solid State Nucl. Magn. Reson., 68-69 (2015) 37-56.
[166] E.S.M. Blaakmeer, G. Antinucci, A. Correa, V. Busico, E.R.H. van Eck, A.P.M. Kentgens, Structural Characterization of Electron Donors in Ziegler–Natta Catalysts, J. Phys. Chem. C, 122 (2018) 5525-5536.
[167] E.S.M. Blaakmeer, G. Antinucci, E.R.H. van Eck, A.P.M. Kentgens, Probing Interactions between Electron Donors and the Support in MgCl2-Supported Ziegler–Natta Catalysts, J. Phys. Chem. C, 122 (2018) 17865-17881.
[168] A. Yakimov, J. Xu, K. Searles, W.-C. Liao, G. Antinucci, N. Friederichs, V. Busico, C. Copéret, DNP-SENS Formulation Protocols To Study Surface Sites in Ziegler–Natta Catalyst MgCl2 Supports Modified with Internal Donors, J. Phys. Chem. C, 125 (2021) 15994-16003.
[169] A.V. Yakimov, D. Mance, K. Searles, C. Copéret, A Formulation Protocol with Pyridine to Enable Dynamic Nuclear Polarization Surface-Enhanced NMR Spectroscopy on Reactive Surface Sites: Case Study with Olefin Polymerization and Metathesis Catalysts, J. Phys. Chem. Lett., 11 (2020) 3401-3407.
[170] E. Morra, E. Giamello, S. Van Doorslaer, G. Antinucci, M. D'Amore, V. Busico, M. Chiesa, Probing the coordinative unsaturation and local environment of Ti3+ sites in an activated high-yield Ziegler-Natta catalyst, Angew. Chem. Int. Ed., 54 (2015) 4857-4860.
[171] A. Piovano, K.S. Thushara, E. Morra, M. Chiesa, E. Groppo, Unraveling the Catalytic Synergy between Ti3+ and Al3+ Sites on a Chlorinated Al2O3: A Tandem Approach to Branched Polyethylene, Angew. Chem. Int. Ed., 55 (2016) 11203-11206.
[172] L. Podvorica, E. Salvadori, F. Piemontesi, G. Vitale, G. Morini, M. Chiesa, Isolated Ti(III) Species on the Surface of a Pre-active Ziegler Natta Catalyst, Appl. Magn. Reson., 51 (2020) 1515-1528.
[173] A. Ashuiev, M. Humbert, S. Norsic, J. Blahut, D. Gajan, K. Searles, D. Klose, A. Lesage, G. Pintacuda, J. Raynaud, V. Monteil, C. Copéret, G. Jeschke, Spectroscopic Signature and Structure of the Active Sites in Ziegler–Natta Polymerization Catalysts Revealed by Electron Paramagnetic Resonance, J. Am. Chem. Soc., 143 (2021) 9791-9797.
[174] E. Morra, G.A. Martino, A. Piovano, C. Barzan, E. Groppo, M. Chiesa, In Situ X- and Q-Band EPR Investigation of Ethylene Polymerization on Cr/SiO2 Phillips Catalyst, J. Phys. Chem. C, 122 (2018) 21531–21536.
[175] J.A. Chudek, G. Hunter, G.W. McQuire, C.H. Rochester, T.F.S. Smith, 29Si magic-angle spinning NMR study of Phillips catalysts: multi-exponential spin–lattice relaxation resulting from adsorption of paramagnetic chromium species onto a silica surface, J. Chem. Soc., Faraday Trans., 92 (1996) 453-460.